Feasibility of particle reinforcement in the casting of a ductile iron gate valve

JS Louw

orcid.org/0000-0003-3890-9554

Dissertation submitted in partial fulfilment of the requirements for the degree *Master of Engineering* in Mechanical Engineering at the North-West University

Supervisor: Prof J Markgraaff

Graduation May 2018

Student number: 23510633

PREFACE

This study was made possible through the cooperation and support of various individuals and organisations to whom I owe my deepest gratitude. I want to use this opportunity to thank them.

Thanks to:

God, for making me capable and teachable, and for undeservingly blessing me with countless opportunities and the individuals mentioned below.

Professor J. Markgraaff for fuelling my interest in metallurgy and for firm guidance and persistence.

Brian Clough from Ceramic & Alloy Specialists for insight, assistance, kindness and provision of the constituents used in this study.

Pierre Rossouw from CSIR for patience, insight, assistance, and equipment used in the melting and casting done in this study.

Vaal University of Technology for the manufacturing and provision of the additive manufactured sand mould used in this study.

Ash Resources for the provision of fly ash samples used in this study.

Mr. Sarel Naudé and Mr. Thabo Diobe at the Mechanical Engineering Laboratory, for technical assistance and testing equipment.

My friends for support, prayers and motivation throughout this study.

My parents and brothers for unwavering support, prayers, and understanding.

KEYWORDS

Cast Iron reinforcement

Compo-casting

Ductile Iron

Dispersion Strengthening

Fly Ash

Metal Matrix Composite

Particle Reinforcement

Stir Casting

Semi-solid

Wetting

ABSTRACT

Feasibility of particle reinforcement in the casting of a ductile iron gate valve.

The mining industry relies on gate valves to shut off flow in pipe systems. The demand for, specifically, ductile iron valve housings is steadily increasing in mining applications where cost, wear, and corrosion is a concern.

The South African iron and steel industry faces several challenges as the number of foundries in the country have experienced a decline of 22%, where 24 foundries have closed down between 2007 and 2014. To increase global competitiveness of small foundries the cost and thus cast iron volumes used in the casting of gate valves must be reduced. Reduced volumes of cast iron, used in the casting of valve housings, will inevitably result in thinner wall thicknesses and the more likelihood of failure, due to reduced strength.

In this study strengthening mechanisms of ductile iron in thin walled castings have been reviewed; and the feasibility of an appropriate casting method, based on a strengthening mechanism, have been tested. In similar studies, strengthening of metallic alloys have been achieved through dispersion of particles in a matrix, through the method of compo-casting; however, little research has been done on further improvement of cast iron. Fly ash, a by-product of coal fired power stations, is an abundant resource, and have been used, in recent studies, to, successfully, improve mechanical properties, such as the tensile strength, impact strength, wear resistance, and hardness of aluminium alloys.

The aim of this study was to improve the strength of SG42 ductile iron, through the incorporation of fly ash particles, using conventional casting methods. Compo-casting was used as casting method wherein 0.8 wt% of fly ash particles were added to the melt, the melt was stirred, and cast, in the semi-solid phase, to improve the wetting of the particles by the melt and obtain a homogenous casting.

Through the examining of fracture surfaces, by scanning electron microscopy, it was found that wetting of the fly ash particles were not sufficiently improved to successfully achieve the necessary strengthening mechanism. As a result, the tensile strength of the fly ash reinforced ductile iron experienced a decrease. The impact strength experienced a decrease through the addition of fly ash particles to the matrix. Further it was found that the porosity of castings increased as a result of semi-solid casting.

TABLE OF CONTENTS

LIST OF ABBREVIATIONS

ASTM	American Society for Testing and Materials
CSIR	Council for Scientific and Industrial Research
MMC	Metal Matrix Composite
SiC	Silicon Carbide
SG	Spheroidal Graphite
UTS	Ultimate Tensile Strength
SG42	Spheroidal Graphite iron with a UTS of 420 MPa
RE	Rare Earth Elements
FeSi	Ferrosilicon
Al_2O_3	Alumina
SEM	Scanning Electron Microscope(y)
J	Joule
CM	Casting Method
RPM	Revolutions Per Minute
wt%	Weight Percentage

LIST OF FIGURES

LIST OF TABLES

Chapter 1

Introduction

1.1 Background

Industries such as mining, pharmaceutical processing, water provision in towns and cities, and petroleum all rely on three main transporting methods namely, road, rail, or pipe systems to transport fluids or gasses. The means of transport are somewhat similar in that they require valves to control and facilitate flow of inventory in either direction. The mining industry rely especially on gate valves to shut off flow in pipe systems, where the valve either restricts or allows the flow of a fluid, through the housing, by lifting a round or rectangular wedge or gate out of the path of a fluid.

Valve housings are usually cast from metallic alloys, but the demand for, specifically, ductile iron valve housings is steadily increasing in mining applications where cost, wear, and corrosion is a concern. The range of service of ductile iron valve housings is comparable with cast steel valves and is preferred to cast steel valves in especially steam supply pipelines, and high pressure gaseous applications.

The distinctive nodular graphite formation of ductile iron, contributes to the significant increase in, especially, ductility. As engineering material, ductile iron exhibits a high elastic modulus, mechanical strength, corrosion resistance, and fatigue resistance in addition to toughness and machinability. It's low cost and ease of production contributes to ductile iron being a widely used structural material in valve casting (Tânia Nogueira Fonseca Souzaa *et al*., 2014, Ductile Iron Society, 1998).

The South African iron and steel industry faces several challenges as the number of foundries in the country have been on the decline since 2003. The total number of foundries have decreased from 270, in 2003, to 265, in 2007, to a further 170, in 2014. The number of ferrous foundries have experienced a decline of 22%, where 24 foundries have closed down between 2007 and 2014. As economic, labour, and environmental challenges constrain foundries in South Africa, measures are necessary to increase the level of global competitiveness. In some foundries with smaller scale production, an opportunity of flexibility and engineering versatility now arises, where smaller production runs and innovation are now possible without great losses (J.T. Davies, 2015). One of the obvious methods to increase global competitiveness of small foundries is to reduce the cost of gate valves. The cost, in turn, can be reduced by reducing the volume of cast iron used in the housing of the valve.

1.2 Problem Statement

The problem is that reduced volumes of cast iron, used in the casting of valve housings, will inevitably result in thinner wall thicknesses and the more likelihood of failure, due to reduced strength. Accordingly, the structural strength of thin walled cast iron valve housings needs to be improved.

1.3 Aim

The aim of this study is to review strengthening mechanisms to maintain and improve the structural strength of ductile iron in thin walled castings; and to test the feasibility of an appropriate casting method based on a strengthening mechanism.

Chapter 2

Literature study

2.1 Nomenclature

2.1.1 Composition of Cast Iron

Cast iron is an iron-carbon alloy containing a minimum of 2% carbon, and in varying percentages, silicon, sulphur, phosphorus, and manganese, in a total of up to 10%. The low cost of cast iron can be attributed to the use of pig iron, having a low production cost with no considerable expensive refining processes (R.A. Higgins, 1993). Different grades of pig iron are used as base material from which the cast iron is made up of, by adding elements in different ratios and combinations to achieve a composition that promote certain desired properties.

Basic properties of cast iron include rigidity, high compressive strength and wear resistance. The composition of cast iron can be tailored to promote properties of machinability, good fluidity during casting, a reduced melting point, hardness, and ductility. Cast iron is generally classified into different classes according to the presence of carbon as either, graphite or iron carbide (cementite) in the resulting structure. Cementite often attributes to a hard and brittle casting (R.A. Higgins, 1993), while the presence of carbon in the form of graphite can have varying effects, depending on its shape.

Elements such as phosphorous, silicon and manganese tend to be graphitising elements. Silicon is known to dissolve in the ferrite of cast iron and increases the instability of cementite, thus favouring the formation of graphite. Phosphorus and silicon, present in specified amounts, increases the fluidity of a cast iron melt and improves casting properties. Excessive presence of these elements, however, result in an increase of a hard and brittle iron. Manganese stabilises carbides, however, the presence of sulphur causes the manganese to reduce the sulphur content and have a graphitising effect (R.A. Higgins, 1993).

The tendency of magnesium, chromium, and sulphur is to promote the formation of cementite in a melt (R.A. Higgins, 1993). These elements, depending on the type of iron that is manufactured, are necessary in that sulphur react with oxygen and magnesium to act as nucleation sites on which graphite can nucleate. The ratio of sulphur to manganese is considered important as this can favour either nucleation sites for graphite or promote the formation of carbides (Svein Oddvar Olsen *et al*., 2004).

2.1.2 Nucleation of Graphite

In cast iron, dissolved carbon precipitates in the form of either cementite or graphite. Primary austenite solidifies first in a hypo-eutectic grey iron, causing the remaining iron in the melt to grow richer in dissolved carbon. With a small degree of undercooling graphite starts to precipitate in flake-like structures in the iron matrix (W. Maschke and M. Jonuleit). A slight increase in undercooling results in further graphite precipitation resulting in branching of graphite nuclei. A significant increase in undercooling, or quenching, will suppress the formation of graphite and instead cause cementite to precipitate (R.A. Higgins, 1993).

Cast iron is inoculated to introduce nuclei in the melt on which graphite can nucleate with a low degree of undercooling, increasing the number of graphite nuclei and have branching occur earlier in the solidification process, resulting in fewer cementite nuclei in the final solidified structure. Consequently, the final structure will naturally contain more ferrite or austenite. A greater degree of undercooling allows the nucleation of a greater number of smaller eutectic cells. This promotes the formation of graphite flakes, that are randomly oriented (American Society for Materials) and preferred for most applications (R.A. Higgins, 1993, Svein Oddvar Olsen *et al*., 2004).

Magnesium and cerium are known carbide promoting elements, however, these elements are necessary in the case of a ductile iron to transform graphite to spherical nodules. As in the case of manganese, graphite nucleates as the presence of sulphur (H. J. Grabke *et al*., 2002), decreases in the melt after MgS generally floats to the surface to form slag. The result of the oxides and sulfides, of magnesium, in the slag is a decreased residual magnesium (Ductile Iron Society, 1998) content in the melt to, not much higher than, 0.04%, acting as the nucleating and nodulising magnesium content. The precipitation of graphite is transformed from a dendritic or flake structure, found in grey iron, to a nodular structure, required in ductile iron by this remaining magnesium content.

2.1.3 Rate of Cooling

During the solidification of cast iron, the rate of cooling significantly effects, at first, the grain size. Sufficient undercooling allows the melt to form crystals at nucleation sites in the melt, usually provided by the inoculant or other impurities in the melt. Once nucleated, a crystal will grow until its boundaries interfere with neighbouring crystals. In this way, greater undercooling result in a finer grain size. In addition, the rate of cooling during solidification effects the final microstructure of the casting. Castings are known to have varying crystal sizes from the edge to the centre of a casting, where a much finer grain size is expected in areas subjected to either the mould surface

or air, with a larger degree of undercooling. The formation of cementite is favoured in such areas, resulting in a white, hard, and brittle structure (R.A. Higgins, 1993).

In cast iron components, this is an important consideration, as thin sections will be subject to the formation of cementite, as shown in Figure 1, or, at best, pearlite, suppressing the formation of graphite. The result is a white cast iron without beneficial mechanical properties of either, grey or ductile iron. Thin sections are therefore more susceptible to brittle fracture, due to rapid cooling. Thin sections composed of ductile iron displays graphite nodules, due to the presence of magnesium, however, here, dissolved carbon prefer to form iron carbide, thus forming less, and smaller graphite nodules.

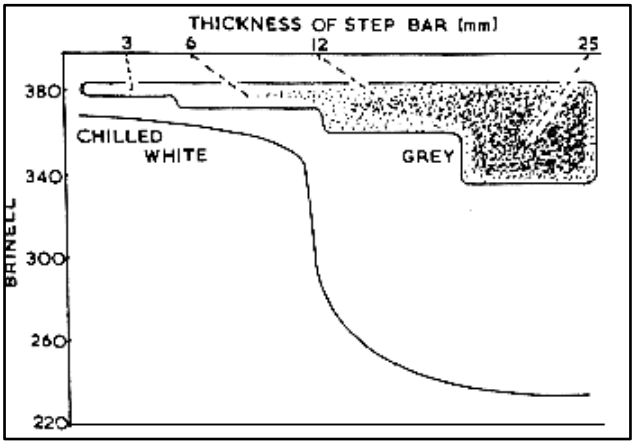

Figure 1: A graph, modified after Higgins (1993), showing the increase in Brinell hardness with a decrease in section thickness, due to the formation of cementite.

2.1.4 Ductile Iron

The natural tendency of graphite in cast iron is to be present in flake-like structures acting as wide faced discontinuities. Graphite flakes exhibit sharp edges creating areas of high stress concentration resulting in crack propagation. This is revealed by the grey fracture surface exhibited by grey iron (American Society for Materials, 1996), indicating fracture along graphite flakes. Although cast iron, in general, is known for relatively brittle behaviour, a significantly more ductile behaviour can be obtained with the addition of nodulising elements such as magnesium or cerium. As mentioned, these elements cause the transformation of graphite from a flake to a nodular or spheroidal structure, eliminating stress raisers and resulting in a less separated matrix (R.A. Higgins, 1993). Ductility in ductile irons, or spheroidal graphite (SG) irons, is a result of

spherical nodules of graphite in the matrix that act to distribute localised stress reducing the probability of crack propagation and fracture.

Foundry practice for most ductile irons comprise of magnesium or cerium (R.A. Higgins, 1993) treatment to achieve nodularity of graphite. ELKEM ELMAG 7311 ®™ magnesium noduliser is a typical product introduced to a base metal to achieve nodularity. Magnesium is highly reactive at elevated temperatures, combining mostly with oxygen (W. Estes James and E. Spangler Grant 1959) and sulphur in the melt in a highly exothermic reaction. Ideally, the magnesium addition of a ductile iron should not exceed 0.06% as the recovery of magnesium is very limited. To achieve a good nodular graphite structure, at least 0.04% magnesium should be present.

The composition of ductile iron is further modified from that of grey iron in that the silicon content is increased to counter the carbide forming tendencies of nodulising elements in especially thin sections. The production of SG irons require a composition specific charge “as free as possible from carbide stabilizing elements” (R.A. Higgins, 1993). The result is an iron with an as cast tensile strength of up to 900Mpa, characterized by high ductility and toughness, in the case of a ferrite matrix, where a pearlite matrix generally gives rise to strength (Ductile Iron Society, 1998).

Ductile iron is usually inoculated just prior to casting with a silicon-containing alloy. An inoculant ELKEM Zircinoc ®, containing zirconium, can be introduced to the melt with the purpose of forming specifically oxides and sulfides that are more stable than that of MgO and MgS, not floating immediately, but, ideally, remaining in the melt, acting as definite nucleation sites for graphite.

2.2 Strengthening Mechanisms

2.2.1 Mechanical Deformation

Plastic deformation in a metal occurs when the applied stress exceeds the critical yield stress. Stress applied on a metal is translated to a shear movement and stress in the lattice. Motion along crystallographic planes (slip) is a prominent mechanism of plastic deformation in metals. The imperfection of crystalline materials allows defects to be present in the crystal structure and thus limit, particularly, the strength. Dislocations are defects in the crystal structure that act as carriers of deformation since a metal is prone to deform plastically along a plane in which dislocations exist, as shown in Figure 2. Cumulative movement of these dislocations leads to gross plastic deformation. Dislocation motion involves the breaking and reformation of inter-

atomic bonds (P.S.V. Kailas) and result in plastic deformation, as shown in Figure 3, at lower levels of stress than the documented yield stress.

Dislocation movement of atoms occur along a slip plane, where the applied force exceeds the strength of the bonds along this plane. Atoms on the slip plane generally produce a step by moving the same distance along the slip plane. In crystalline systems, atoms along a slip plane contribute to other bonds in the lattice that are not in the slip plane and thus not dislocated by the movement. It is important to note that prior to the existence of slip, the metal had undergone some preceding amount of elastic deformation. During elastic deformation, rearranging of atoms, along the slip plane, have not yet occurred and existing dislocations have not moved, however there exists some tensile stress, caused by shear movement, between bonds. This same shear movement is experienced by bonds neighbouring, what is to become, the slip plane and is merely a result of the tensile stress in this plane, transferred to neighbouring planes. The effect of this movement is decreased as the distance from the slip plane is increased.

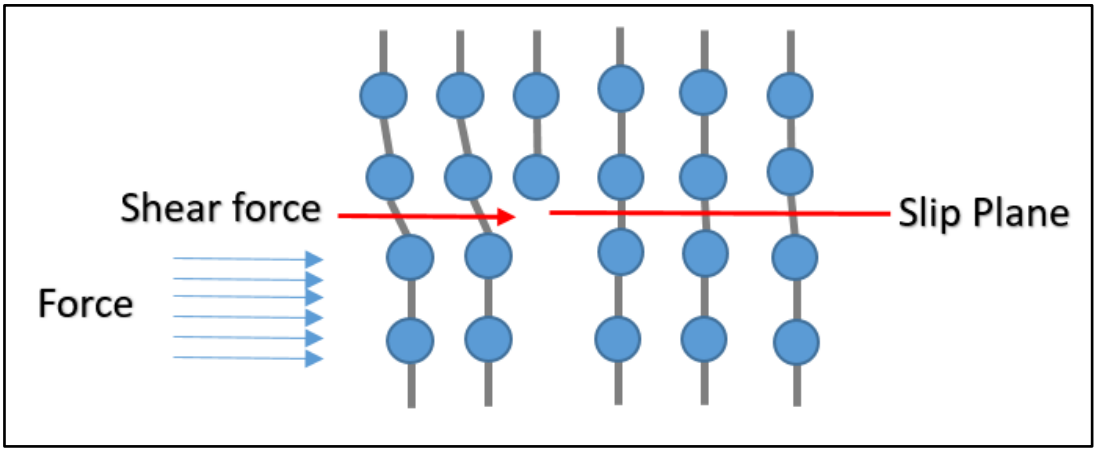

Figure 2: A depiction of the formation of a slip plane in a defective crystalline lattice, prior to deformation.

In the case where the critical yield stress of the composite is exceeded, motion of the slip plane occurs. Particles with sufficient strength will not allow the slip plane to penetrate, but rather force the slip plane to bend around it as unhindered parts of the plane advances through the lattice. Sections in which the slip plane is completely prevented from advancing, will reveal dislocation loops around inclusions.

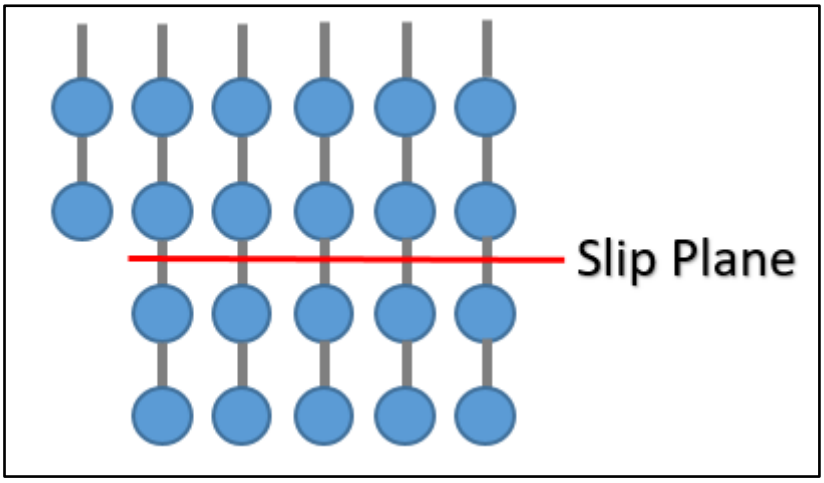

Figure 3: A depiction of a deformed and rearranged crystalline lattice due to dislocation motion.

2.2.2 Phase Transformations

Further strengthening on ductile iron can be brought about by phase transformation applied through heat treatment. An increase in mechanical properties such as toughness and ductility can be observed through a ferritizing annealing heat treatment, in turn, normalizing at an austenitizing temperature will give rise to properties such as strength and ductility, resulting from the close packed face centred cubic cells of the austenitic phase (American Materials Society, 2008). By austenitizing and sufficiently quench hardening ductile iron, to obtain a martensitic matrix, maximum hardness can be obtained, in addition to a tensile strength of up to 1380MPa, compared to a tensile strength in the range of 400MPa for ductile iron exhibiting a ferritic matrix (Ductile Iron Society, 1998).

Modifications and improvements of ductile iron through phase transformations is a relatively familiar trait in that its possibilities are well known. This mechanism, however, tend to favour some properties at the cost of another. As in the case of ductile iron, when heat treatment is applied to give rise to hardness, the result is a hard and relatively brittle structure with a decrease in impact strength.

2.2.3 Precipitation Hardening

Precipitation hardening is a method of strengthening usually applied to supersaturated solid solution alloy systems. For precipitation hardening to be considered as strengthening mechanism in an alloy system, the solubility limit should decrease with a decrease in temperature (T.

Szykowny *et al*., 2014). Thus, the solubility of the precipitating element must increase with an increase in temperature.

During precipitation hardening heat treatment, an alloy is solution heat treated, to induce one or more constituents to enter into solid solution, and then quenched to suppress the separation of the constituent to remain in solution and exist in an unstable supersaturated state at a low temperature. Through ageing, precipitation of the alloying element occurs through a nucleation process (R.E. Smallman, 2013). T. Szykowny *et al*. (2014) subjected a spheroidal cast iron with additions of 0.51% Cu and 0.72% Ni to precipitation hardening. The study obtained a 13.2% increase in hardness after a five-hour ageing process of pre-normalised cast iron.

2.2.4 Solid Solution Strengthening

Solid solution strengthening is a common strengthening mechanism, in metals, wherein alloys are formed with specific elements to achieve strengthening through obstructions in a lattice. Solid solution strengthening is done during casting where a solute metal is dissolved in a solvent metal in the liquid phase. Two kind of solid solution systems exist namely a substitutional solution, shown in Figure 4, and an interstitial solution, shown in Figure 5.

A substitutional solution is a system in which atoms of the solute replace atoms of the solvent in the crystal lattice. A difference in the size of the atoms, causes the interruption of the regularity of the lattice. Dislocation motion is thus obstructed by the substitutional atom.

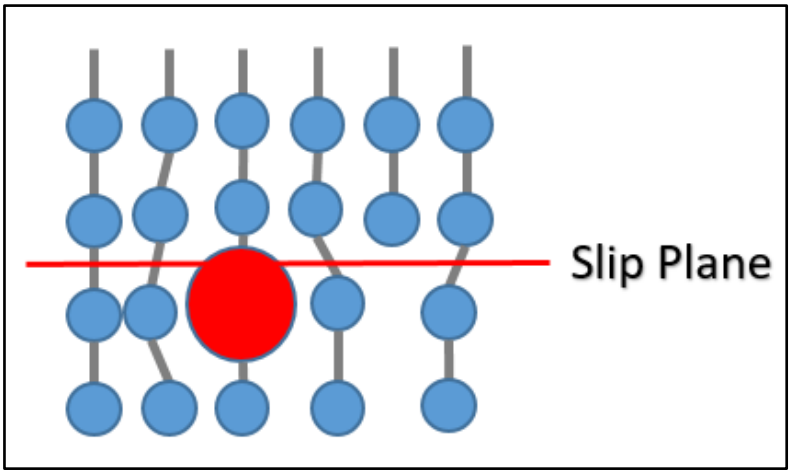

Figure 4: A depiction of a crystal lattice in a substitutional solid solution system with the presence of a dislocation and proposed slip plane.

Interstitial solid solutions are formed through the ability of a solute atom to fit into the interstices of the lattice of a solvent (R.E. Smallman, 2013). The interruption of the crystal lattice obstructs dislocation motion by distributing localised stress from the slip plane to surrounding planes in the lattice. An interstitial system of solid solution strengthening is well described by the presence of carbon in steel or cast iron. However, further solid solution strengthening of a ductile iron was achieved by A.Ş. VeSan (2012) through the solid solution strengthening of a ferrite matrix by silicon.

Improved mechanical properties were reported with a linear relation between tensile and yield strength for a silicon content up to 4.3%. A further increase in silicon content resulted in a "sudden drop in elongation" and brittle behaviour of the material.

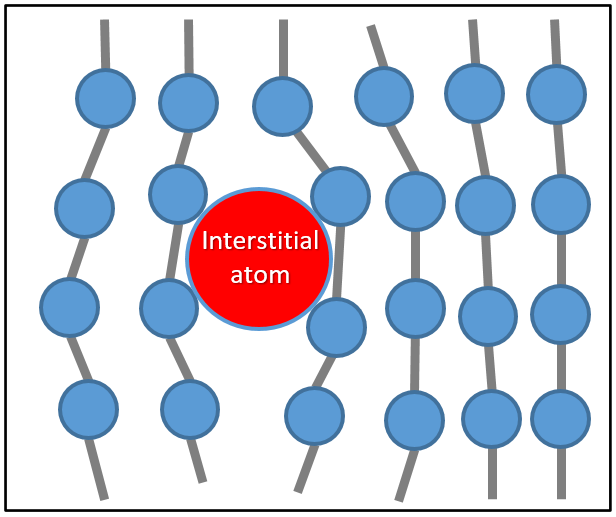

Figure 5: A depiction of the disruption of a crystal lattice containing an interstitial atom in an interstitial solid solution system.

2.2.5 Dispersion Strengthening

Particle dispersion strengthens on the principle of inhibiting dislocation and grain boundary motion (S. Vorozhtsov *et al*., 2016). Hindrances to dislocation motion is typically employed through interstitial atoms, foreign particles, grain boundaries, and phase changes. The existence of particles, acting as an inclusion between rows of atoms in the lattice, causes the shear stress, that may occur in one plane, to be transferred to the particle and further to a number of planes, as shown in Figure 6.

The mechanism of strengthening is similar to that of precipitation hardening, wherein a larger fraction of the applied stress is still carried by the matrix, and the dispersed particles act as

hindrances to dislocation motion through the matrix (J.J.A.C. Smit, 2000). This effectively increases the number of bonds that act against the shear stress. As a result, higher stresses are required to move dislocations along the slip plane, in which case more dislocations will be generated, depending on the size of the inclusion (P.S.V. Kailas, S. Suresh *et al*., 1993).

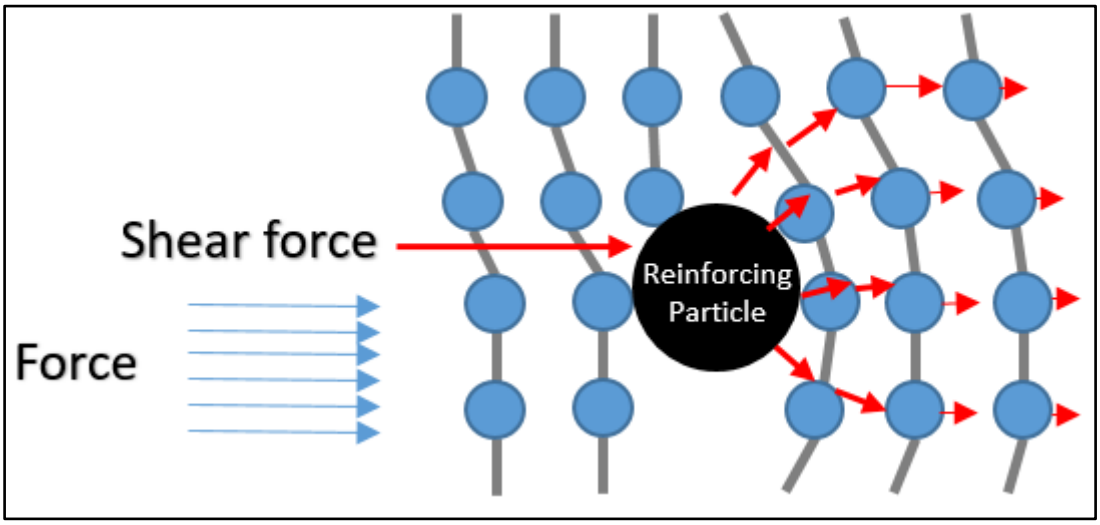

Figure 6: A depiction of a reinforcing particle in a crystalline lattice inhibiting dislocation motion by distributing force to surrounding areas in the lattice.

The manufacturing of particle reinforced MMC's generally adopts liquid state processes (Rajeshkumar Gangaram Bhandare and P.M. Sonawane, 2013). When focussing on particulate reinforcement in general, the rheological behaviour of the matrix melt, incorporation method, interactions between the reinforcement and matrix, before, during and after mixing, and the changing particle distribution during solidification (Abhijit Dey and Krishna Murari Pandey, 2015) are all major areas of concern as distribution and orientation of the reinforcement particles in the matrix are influenced, and largely determine the mechanical properties and consistency of the composite.

2.3 Particle Reinforcement

Strengthening, of especially metals, through dispersion of foreign particles in liquid state processes is a familiar strengthening mechanism in the field of metal matrix composites (MMC's). The application of such MMC's in fields such as the aerospace, automotive, and the electronics industries (A.P.M. Franck A Girot, Tsu Wei Chou) have been on the increase since new innovations led to better performing materials becoming less expensive.

The development of particle reinforced MMC's have seen attempts of various particles being used to strengthen a metal matrix. H. KHOSRAVI *et al*. (2013) successfully incorporated SiC particles into an aluminium alloy matrix which resulted in increases in the tensile characteristics of the metal. An increase in tensile properties was also observed by M. Kok (2005), together with an increase in hardness with the incorporation of varying sizes of Al_2O_3 particles into an 2024 aluminium alloy matrix.

A.C. Reddy (1998) used titanium carbide nanoparticles to reinforce an aluminium 2024 alloy of which the interface between particles and the matrix, together with the fracture of particles were evaluated. Results indicated an increase in the tensile elastic modulus with an increase in titanium carbide particles in the melt. The tendency of particle fracture was to increase with an increase in particles in the matrix.

Fly ash proves to have potential as reinforcement in MMC's in areas with economic considerations. As a by-product of coal combustion, fly ash particulates, apart from being proven to have improved desired mechanical properties, has the potential to reduce the cost of MMC's, especially when compared to the cost of incorporating other particles such as SiC, Al_2O_3, graphite, etc.

Particles of fly ash are generally classified into two types namely, cenosphere and precipitator. Cenosphere particles are hollow with a density of less than 1.0 g/cm^3, while the solid spherical particles, with a density in the range 2.0-2.5 g/cm^3, are precipitator fly ash (Abhijit Dey and Krishna Murari Pandey, 2015). Cenosphere fly ash particles are generally utilised for the fabrication of ultra-light composite materials, whereas precipitator fly ash particles have proved to improve strength, stiffness and wear resistance of selected matrix materials. These improvements can be attributed to the spherical shape of precipitator particles, acting as obstructions in slip planes in a lattice, distributing shear stress onto several other planes, ultimately obstructing dislocation.

X Liu and M Nilmani (1996) fabricated an aluminium-fly ash metal matrix composite, using an A380 aluminium alloy. A low cost full liquid route was used in the production of the composite on which the effect of particle volume fraction on the mechanical properties of an aluminium-fly ash MMC was to be determined. The results indicated a decrease in both the hardness and ultimate tensile strength of the composite, with an increase in volume fraction of microspheres. The decrease in these mechanical properties were attributed to the presence of porosity and debonding between the microspheres and the aluminium matrix. However, with the composite density being 15-20% lower than the matrix alloy, the strength to weight ratio of the fly ash MMC is similar or marginally increased.

The influence of the incorporation of fly ash on the microstructure of the resulting composite was determined using optical and SEM photomicrographs. The microstructure of the cast aluminium alloy depicts a dendritic structure caused by solidification at a high cooling rate. The effect of the fly ash in the matrix is evident as the resulting microstructure of the cast MMC shows refinement of the dendritic structure. It is believed that the solidification pattern leads to the refinement of grains due to both the resistance the fly ash particles offer against the growing of α-aluminium grains during solidification, and the ability of fly ash particles to act as nucleation site. As the content of fly ash particles increases, the number of nucleation sites are increased. The fly ash particles thus serve the additional purpose of an inoculant.

K.V. Mahendra and K. Radakrishna (2007) fabricated and characterised a fly ash reinforced Al-4.5%Cu alloy metal matrix composite, using stir casting. In order to create a vortex, the molten metal was stirred at 600 rpm prior, and during the introduction of the particles into the melt. Prior to the slow addition of varying percentages, of 5-15wt%, fly ash particles into the melt, the particles were preheated to an undisclosed temperature. 0.5wt% magnesium were added to the molten metal to promote wetting of the particles by the melt. After casting, the composites were cooled at room temperature.

Several tests were performed on the composite, determining the mechanical and slurry behaviour. From the results it was observed that both the fluidity length and density of the composite decreased with an increase in the percentage of fly ash particulates. The microstructure of the MMC reveals a uniform distribution of fly ash in the matrix, with no voids or discontinuities and good bonding between the fly ash particle and the matrix material. An increase in the hardness and tensile strength were observed with an increasing percentage of fly ash particles, however, castings with smaller cross sections exhibited higher tensile strengths than those with larger cross sections. This phenomenon is attributed to the finer grain size, which is generally achieved in smaller sections, as a result of faster heat transfer. An increase in the compressive strength and impact strength of the composite is observed with an increase in the fly ash content. The dry sliding wear behaviour of the MMC were analysed and revealed that wear decreases with an increasing fly ash content. Castings with smaller diameters exhibited less wear than castings with larger diameters. The presence of fly ash in the matrix offered a resistance to wear.

The incorporation of fly ash particles into metal matrices, as have been done in Al-7Si-0.355Mg alloys (T.P.D. Rajan *et al*., 2007) , are of great potential in the manufacturing of metal matrix composites. The use of fly ash as reinforcement is an attractive concept with beneficial properties such as being a low-density and low-cost reinforcement with high availability. Constituents of fly ash (alumina-silicate) includes SiO_2, Al_2O_3, Fe_2O_3 and CaO; whereby the incorporation of its particles into an aluminium matrix potentially improves the wear resistance, hardness, stiffness,

and damping properties. As in the case of Al_2O_3 particles, compounds in the form of oxides compromises the ability of a melt to wet the surface of fly ash particles. Previous studies have revealed methods, such as particle treatment, to solve the wetting problem between particles and a matrix, however, the interfacial phenomena in MMC's is a recurring problem with different characteristics for every composite.

2.4 Interfacial Phenomena

In the production of MMC's, the formation of the interface between the matrix and the reinforcing phase has a substantial influence on the manufacturing method and resulting composite characteristics (K.U. Kainer, 2006), as the interaction between the fibre and the matrix determines the adhesion between them; directly influencing the mechanical properties of the composite (L.F. G. Chadwick).

Considering the fibre-matrix interface, two problems generally arise in the manufacturing of MMC's, namely interfacial reactions and wettability. The importance of Interfacial phenomena is highlighted in cases where the reinforcement and matrix are chemically unstable and react to form undesired third phases. High interfacial reactivity can be countered by minimizing the exposure to, what is regarded as, elevated temperatures, relative to the present constituents, during processing. In doing this, the extent of interfacial reactions can be monitored and kept within relatively acceptable limits (L.F. G. Chadwick). In cases of sufficient chemical stability, the reinforcement and the metal matrix can be combined and processed while the metal matrix is in the liquid or semi-solid state.

Another occurrence in MMC production, although related to interfacial reactions, is the lack of wetting of the surface of the reinforcing phase by the matrix. Wettability is generally described as the attempt of a solid to form a common interface with a liquid that comes into contact with it. The extent to which a reinforcement phase is wetted by a metal melt can be determined from the sessile drop technique where a drop of the molten metal is allowed to rest on a flat surface (K.U. Kainer, 2006) of the substrate of the reinforcing phase, at a fixed temperature.

Wetting is characterized by the contact angle between the droplet and the substrate surface, as shown in Figure 7. Applicable to three-phase systems in thermodynamic equilibrium, containing pure liquids and ideal solids, Young's equation states that the contact angle (θ) of a liquid on an ideal solid surface is defined by the mechanical equilibrium of the drop under the action of three interfacial tensions; the liquid's surface tension (γ_{lv}), the interfacial tension (γ_{sl}), and the surface

free energy of the solid (γ_{sv}) (Y. Yuan and T.R. Lee, 2013). An angle > 90° describes a non-wetting system where an angle < 90° describes wetting system (S.T. Mileiko).

$$\gamma_{sv} = \gamma_{sl} + \gamma_{lv} \cdot cos\theta$$

A chemical approach into the interfacial phenomena is legitimate as far as interfacial reactions are concerned. A chemical approach, however, only addresses part of the problem of wettability. When focussing on the manufacturing of MMC's by infiltration of a preform, made of the reinforcing phase, capillary phenomena are also of interest. Pressure infiltration have often been used, with success, to decrease the contact angle, resulting in sufficient wetting and adhesion between the phases. Pressure infiltration can however not be applied to particle dispersion strengthened systems. These systems require liquid stirring processing methods that have in some cases resulted in decreased mechanical properties of the composite, which have been attributed to particle-matrix de-bonding; a result of a lack of wetting and adhesion during manufacturing (L.F. G. Chadwick).

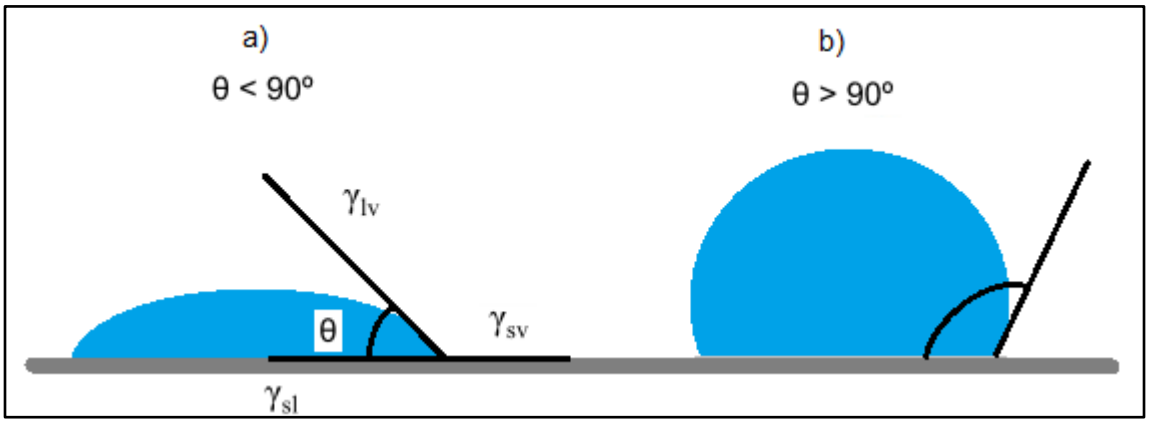

Figure 7: A representation of a droplet resting on a substrate surface in a a) wetting and b) non-wetting system.

The existence of the problem of wettability have brought about changes in the production and constituent selection of MMC's. Apart from having a specific manufacturing technique for different types of MMC's, alterations can be brought about to increase the compatibility of the constituents of which the composite comprises.

2.4.1 Improvement of Wetting

Achieving good wetting between the matrix and the reinforcement have in some cases been found to be associated with the degree of reactivity between them; as well as the tenacity of the oxide layer on (S.T. Mileiko, L.F. G. Chadwick), especially, aluminium. Alloying additions in the matrix

material effects, predominantly, the wetting angle at the fibre matrix interface, but also the ease of infiltration of preforms. Some additions promote reactions at the interface, however these reaction promoting additions tend to lower the wetting angle between the substrate surface and the matrix, thus enhancing wetting.

The wetting process is kinetic and dependent on time, temperature, and pressure. Karl Ulrich Kainer (2006) conducted an experiment, measuring the degree of wetting and the temperature dependence thereof, of different aluminium alloy compositions on SiC plates. The effect of alloying elements on the wetting angle is clearly seen; acting by changing the surface tension of the melt or by reacting with the reinforcement. He concluded that the role of interfacial reactions therefor is important as a new system can exist from it and change the interfacial energies. The general tendency, however, of temperature variation is that an increase in temperature enhances wetting.

Alloying additions to the matrix material that do not promote interfacial reactions but disrupt the oxide layer on the reinforcement surface have also proven to be effective and correlate with wetting angle data in the sense that the transition temperature, from a non-wetting system to a wetting system, are decreased with such additions.

A more sophisticated, but relatively expensive and time consuming, technique based on the same principle as alloying additions, is to modify the fibre or particle surface with a coating. In the case of aluminium, for example, coatings that either promote reactions at the fibre-matrix interface or disrupt the oxide layer on the metal surface will improve wetting (L.F. G. Chadwick).

The reinforcement surface can be influenced significantly due to the absorption of mainly oxygen from the atmosphere. Al_2O_3 and graphite particles have often been heat treated prior to incorporation into aluminium melts and improved the ease of incorporation as a result of improved wetting. This was attributed to the desorption of gases from the reinforcement surface during the heat treatment (S.T. Mileiko).

2.5 Applicable Casting Processes

In the manufacturing of MMC's, the phase of the matrix material, during processing, distinguishes three processes through which the production of a MMC can be achieved. These processes include: liquid state processing, solid state processing, and semi-solid, or two phase processing (I.A. IBRAHIM *et al*., 1991). Among these methods, liquid state processes are identified as suitable process engineering methods (K.U. Kainer, 2006) which allow MMC's to be manufactured

through altering existing casting methods (J. Hashim *et al*., 1999). This results in methods that are applicable to and economically feasible for the local material industry.

Liquid state processes largely consist of particle or fibre reinforcement, and include processes in which the reinforcing particles are added to a liquid phase matrix, among which melt stirring is generally accepted as conventional method (Rajeshkumar Gangaram Bhandare and P.M. Sonawane, 2013). It is projected that the cost of manufacturing by means of melt stirring can reduce the cost to approximately one-third to that of other MMC production methods. Large scale production increases the economic feasibility even further, with a projected cost of one-tenth to that of other methods (J. Hashim *et al*., 1999). Such methods include stir casting, compo-casting and a modified compo-casting technique (T.P.D. Rajan *et al*., 2007, H. KHOSRAVI *et al*., 2013). Other more expensive techniques include the manufacturing and metal infiltration of a preform of either continuous fibres or processed whiskers or particles.

2.5.1 Stir Casting

The conventional stir casting process comprises of both, the addition of the reinforcement particles, and the casting process itself being done in the fully liquid state of the melt (S. AMIRKHANLOU and B. NIROUMAND, 2010). M. Ramachandra and K. Radhakrishna (2007) studied the effect of fly ash as reinforcement (up to 15 wt%) on sliding wear and corrosive behaviour in an Al-Si (12%) matrix. The reinforcing fly ash particles contained both precipitators and cenospheres. The MMC used in the study was prepared using a stir casting technique, wherein the fly ash particulates were preheated to around 600°C prior to being added to the molten metal. Once the fly ash particles were added to the molten metal the mixture was stirred continuously with a mechanical stirrer at 720°C for 5-8 minutes at 550 rpm.

In order to increase the wettability of the fly ash particles, small quantities of magnesium were added during stirring. The pouring temperature was maintained at 680°C, where after the melt was allowed to solidify in the mould. It was concluded that an increase in reinforcement increased the wear resistance and reduce the coefficient of friction. The 20-30% increase in wear behaviour was attributed to its superior load bearing capacity. A decrease in corrosive behaviour was observed in reinforced samples. Another study by M. Ramachandra and K. Radhakrishna (2005) focussed on the resulting density, hardness, micro hardness, ductility and ultimate tensile strength of fly ash as reinforcement in an Al-Si (12%) matrix. From the results it was concluded that in the immediate vicinity of fly ash particles, the matrix revealed higher hardness values. Ultimately, the density, corrosion resistance and ductility was decreased with the addition of fly ash particles,

however, mechanical properties such as hardness, ultimate tensile strength and wear resistance of the composite were enhanced.

2.5.2 Compo-casting

A similar process to that of stir casting is compo-casting, which is also fit for application in the manufacturing of particle reinforced MMC's. Different from stir casting, the reinforcement addition and casting process, in compo-casting, is carried out in the semi-solid state of the melt (S.T. Mileiko); however in a more recent modified compo-casting technique, the addition of the reinforcement material is carried out with the melt in the semi-solid phase, while the casting is carried out in the fully liquid state (T.P.D. Rajan *et al*., 2007). The melt is agitated throughout the process, from the liquid state until immediately prior to casting.

Vigorous agitation is necessary for the semi-solid mixture to remain in a fluid state and thus prevent the formation and growth of primary phase dendrites. The thixotropic behaviour of the mixture is useful to prevent the sinking or floating of the reinforcement in the matrix (Shy-Wen Lai and D.D.L. Chung, 1994). In the conventional compo-casting process, reinforcing particles are added to the matrix when it contains roughly fifty percent of the solid phase. The continuous agitation of the mixture prevents the agglomeration (S. AMIRKHANLOU and B. NIROUMAND, 2010) of the particles and promotes wetting by the matrix.

T.P.D. Rajan *et al*. (2007) investigated the effect of three different stir casting techniques on the structure and properties of fly ash particle reinforced Al-7Si-0.35Mg alloy. The different stir casting routes included liquid metal stir casting, compo-casting and modified compo-casting (T.P.D. Rajan *et al*., 2007). The fly ash particles used in the study contained both precipitator and cenosphere particles. Fly ash particles are preheated to 600°C for two hours prior to introduction into the melt. Particles are surface treated in an acidic solution under ultrasonic vibration for 5-10 minutes, filtered and dried in an oven. The preheated particles are added to the melt at a feed rate of 3 g/min and stirred at 600 rpm. Magnesium is added to the matrix in order to address the problem of wetting.

From the results it is found that the incorporation, of untreated fly ash particles, with liquid metal stir casting resulted in the agglomeration of particles, and hence a high level of porosity. The presence of the magnesium in the matrix have not aided in breaking agglomerates. The surface treated particles provided better dispersion and distribution with less agglomeration. The improvement is attributed to the surface treatment of the particles. The ultrasonic surface

treatment broke large agglomerates and removed the finer fly ash particles from the surface of larger particles (T.P.D. Rajan *et al*., 2007).

In the case of the compo-casting process, better dispersion was obtained compared to the liquid metal stir casting process. During this process the higher viscosity of the semi-solid alloy imparts shear forces over the agglomerates and this aids in better separation of the dispersoids. The compo-cast composites exhibit higher porosity levels compared to the liquid stir cast composite. This is attributed to the gas porosity caused by the higher viscosity of the composite slurry. The modified compo-casting process resulted in the best distribution of particles among the processes in the particular study. The advantages realized by the modified compo-casting process are better dispersion of particles, a fine primary aluminium grain size and improved fluidity due to casting above the liquidus temperature.

The study highlights an improvement on the compressive strength of the Al-fly ash composite, processed by the modified compo-cast-squeeze casting method, when compared to the matrix alloy. A decrease in the tensile strength of the composite is observed, which has been attributed to particle fracture and particle matrix de-bonding.

H. KHOSRAVI et al. (2013) studied the effect of the parameters of compo-casting on microstructural characteristics and tensile properties of A356-SiC composites. The alloy used has a broad semisolid range and is thus ideal for semisolid processing. To promote wettability of the particles by the aluminium alloy, an SiO_2 layer was formed on the SiC particles by means of artificial oxidation in air.

After melting the aluminium alloy, at 750°C, and adding the preheated SiC particles, semisolid stirring was carried out using a graphite impeller. The stirring temperature, time, and speed varied. Temperatures ranged from 590 - 610°C, where the time ranged from 10 - 30 minutes and the stirring speed 200 – 600 rpm. The casting was done in a cylindrical steel mould, preheated to 400°C. Standard metallographic procedures were carried out on the resulting samples. The distribution of the particles was characterised by the calculation of the distribution factor F_d, such that:

$$F_d = \frac{S.D.}{A_f}$$

where A_f is the mean value of the area fraction of the SiC particles measured on 100 fields of a sample and S.D. the standard deviation. A smaller value for F_d indicates a more uniform distribution.

The conclusion indicates some optimum compo-casting parameters where a decrease in stirring temperature results in a smaller distribution factor, implying a more homogenous distribution. This can, however, only be said for the semisolid state of the matrix. A less homogenous distribution is obtained by an increase in the temperature within the semisolid range. A more homogenous distribution is obtained with the increase in effective viscosity in the slurry during semisolid stirring, compared to liquid stirring. The increased viscosity restricts the movement of the particles and prevents them from floating. The semisolid phase includes some solid phases contributing to the breaking down of particle agglomerates during stirring. A more homogenous distribution is obtained with an increase in stirring time as some zones are free from SiC particles with a reduction in stirring time.

When considering the stirring speed, an optimum value can be reached. This is concluded since 200rpm and 600rpm stirring speeds included some clusters of particles as well as porosity, especially at 600rpm. At lower stirring speeds, in this case 200rpm, left parts of the matrix unreached with SiC particles. A stirring speed of 400rpm, however provides the most homogenous distribution and less porosity when compared to the other cases. These results can be attributed to the increase in shear forces applied when the stirring speed is increased. An increase in the shear forces within the matrix, during stirring, improves uniformity. The higher stirring speed imposed non-uniformity in the particle distribution which is attributed to the agitation severity of the slurry, resulting in clustering. An increase in porosity of compo-cast samples is a recurring problem, with previous studies obtaining similar outcomes (T.P.D. Rajan *et al*., 2007).

Considering the mechanical properties of the composite, it was found that tensile properties increased with a decrease in the stirring temperature, together with an increase in the stirring time. As in the particle distribution, the tensile properties are at experimental optimum at a stirring speed of 400rpm. As the stirring speed is increased, the tensile properties increases, but reaches some maximum value. From the results it is concluded that, in order to increase both uniformity in distribution and advantageous mechanical properties, stirring must be done at a temperature, above, but rather closer than further from the solidus temperature, at an experimented optimum stirring speed, for a longer period of time, in this case 30 minutes. It is found, however, that porosity increases by increasing the stirring speed, time, and temperature.

Chapter 3

Compo-casting of Composites

This chapter presents the compo-casting that was conducted during this study. From the literature, fly ash particles were selected as reinforcement, to be incorporated into a ductile iron matrix through the method of compo-casting. Raw materials and their compositions are presented where after casting procedures, as employed, are presented. Methods of examining the microstructure are also presented, together with standard tensile and charpy tests as, as conducted on cast samples.

3.1 Charge Calculation

3.1.1 Ductile Iron - SABS 936 (SG42)

Prior to casting, the weight percentages of the melt constituents were calculated to comply with the conventional composition (wt%) of SG42, shown in Table 1. The melt constituents, of which compositions are shown in Table 2, were supplied by Ceramic & Alloy Specialists (Pty.) Ltd. in Boksburg, South Africa.

Table 1: An industrial established composition (wt%) for SG42.

C%	Si%	Mn%	P%	Mg%	S%	Fe%
3.1 - 3.8	2.2 - 2.7	0.15 – 0.3	0.04 Max	0.02 – 0.05	0.02 Max	Balance

The melt constituents, with compositions as listed in Table 2, include:

- Grade RF2 pig iron with composition as shown in Table 2, adhering to Draft International Standard ISO/DIS 9147 (The International Organization for Standardization, 1987, American Society for Materials, 1996),
- Ferrosilicon, added to the melt with the purpose of increasing the silicon content,
- Zircinoc, a zirconium containing inoculant,
- Elmag, the magnesium containing noduliser, necessary to manufacture spheroidal graphite iron.

Table 2: Compositions (wt%) of constituents used to manufacture the SG42 iron used in this study.

Constituent	C%	Si%	Mn%	P%	Mg%	S%	Ca%	Zr%	Al%	Fe%	RE%
RF2 Pig Iron	3.9	0.15	0.03	0.04	-	0.02	-	-	-	Bal.	-
Ferrosilicon	-	73.9	-	0.04	-	0.03	0.06	-	0.45	25.6	-
Zircinoc	-	75.0	-	-	-	-	2.25	1.55	1.25	19.9	-
Elmag	-	46.4	-	-	7.20	-	2.47	-	0.60	41.9	1.20

A Microsoft Excel spreadsheet was compiled to, iteratively, calculate the charge composition of the SG42 iron used in this study. The calculation made use of the constituent compositions in Table 2 and a desired weight percentage value, of each constituent in the SG42 melt. These inputs were used to calculate the percentage of each element that was present in the final melt, together with the percentage contribution from the constituents to each melt element. This was done by using the presence (%) of each constituent in the melt, as a fraction of 100%, and then calculating the presence (%) of each element in a constituent, given in Table 2, as a fraction of the whole melt (100%).

Figure 8 shows the Excel output table as discussed in the previous paragraph. Also included in the output table is a composition (wt%) of the resulting SG42 melt, together with the required or redundant weight percentages of each element. From the output table, the input weight percentages of the constituents were adjusted in order to obtain a better approximation of the desired composition shown in Table 1, and to account for fading of elements such as carbon and magnesium, during melting.

Base Material	Kg	wt%	C%	Si%	P%	Mn%	Cu%	Mg%	Cr%	S%	Fe%	Ca%	Al%	Ba%	Sr%	Zr%
F2 Pig Iron	7.6	96.233	3.755	0.112	0.034	0.029	0.000	0.000	0.000	0.019	92.344	0.000	0.000	0.000	0.000	0.000
FeSi Low Al	0.19	2.407	0.000	1.778	0.001	0.000	0.000	0.000	0.000	0.001	0.615	0.001	0.011	0.000	0.000	0.000
	0	0.000														
		0.000														
Treatment																
Elkem Zircinoc	0.04	0.500	0.000	0.375	0.000	0.000	0.000	0.000	0.000	0.000	0.100	0.011	0.006	0.000	0.000	0.008
Elkem Elmag 7311	0.06	0.800	0.000	0.373	0.000	0.000	0.000	0.058	0.000	0.000	0.345	0.000	0.000	0.000	0.000	0.000
	Kg	wt%	C%	Si%	P%	Mn%	Cu%	Mg%	Cr%	S%	Fe%	Ca%	Al%	Ba%	Sr%	Zr%
SG 42 Analysis	7.8926	100	3.755	2.638	0.035	0.029	0.000	0.058	0.000	0.020	93.404	0.013	0.017	0.000	0.000	0.008
Required/redundant			0.155	0.038	-0.005	-0.121	0.000	0.018	0.000	0.000	-0.146	0.013	0.017	0.000	0.000	0.008

Figure 8: The Excel Spreadsheet showing the weight percentages of constituents and their contributions to elements that are added up to give the composition of the SG42 used in this study.

Table 3 shows the composition of the SG42 iron, that resulted from the charge calculation process, as described in this section, and was used for the reinforced ductile iron casting in this study. As final output, the compiled spreadsheet provided the weight and weight percentage of

each constituent, as shown in Figure 9, that had to be added to the melt in order to obtain the composition in Table 3.

Table 3: The charge composition (wt%) for the production of the SG42 cast iron that was used in this study.

C%	Si%	P%	Mn%	Mg%	Ca%	Al%	S%	Zr%	Fe%
3.8	2.6	0.04	0.03	0.06	0.01	0.02	0.02	0.02	93.4

	Kg	%
F2 Pig Iron	7.60	96.293
FeSi Low Al	0.19	2.407
0	0.00	0.000
0	0.00	0.000
Treatment	Kg	%
Elkem Zircinoc	0.04	0.50
Elkem Elmag 7311	0.06	0.80
0	0.00	0.00
0		
		100.00

Figure 9: An output table obtained from the compiled Excel Spreadsheet, showing the weight percentages of constituents in the melt as a whole, together with their mass equivalents.

Since the pig iron chips are not all equal in weight, the weight of the constituents had to be calculated for each melt according to the weight of the pig iron chips used in the particular melt, adhering to the charge composition established in Table 3. Figure 10 shows the table in which this calculation was made, wherein the blue cell is an input cell for the weight of a pig iron chip, and the grey cells were calculated according to the constituent percentages, calculated in the output table that is shown in Figure 9.

Product	%	Mass	
F2	0.963	10.100	kg
Fesi	0.024	0.253	kg
Zirc	0.005	0.052	kg
Elmag	0.008	0.084	kg
	1.00	10.489	kg

Figure 10: A table obtained from the Excel Spreadsheet, where the blue cell is an input cell, calculating the mass of additions for each melt according to the weight of the pig iron in the melt.

3.2 Characterisation and Selection of Fly Ash

Fly ash used in this study was obtained from Lethabo coal fired power station in the Free State, South Africa. Six samples were provided by Ash Resources (Pty.) Ltd. The samples were analysed visually, using a Quanta 200-3D scanning electron microscope (SEM) at the Microscopy Laboratory of the North West University, South Africa. Samples were checked for impurities and the presence of either cenosphere or precipitator particles. For the purpose of reinforcing, precipitator particles were preferred, as they are near-perfect spherical solid particles and have a higher density than that of cenospheres, which are hollow sphere particles, lowering the risk of particle fracture in the matrix. Two samples were eliminated due to high levels of impurities and a significantly notable difference in particle size distribution from visual analysis. Micrographs A, B, C, and D, in Figure 11, represents the remaining samples and displays mostly precipitator particles, with visible impurities and also larger particles in samples B (DuraPozz) and D (SuperPozz Tailings). The remaining samples, as labelled by Ash Resources (Pty.) Ltd. are:

A. Cyclone
B. DuraPozz
C. SuperPozz
D. SuperPozz Tailings

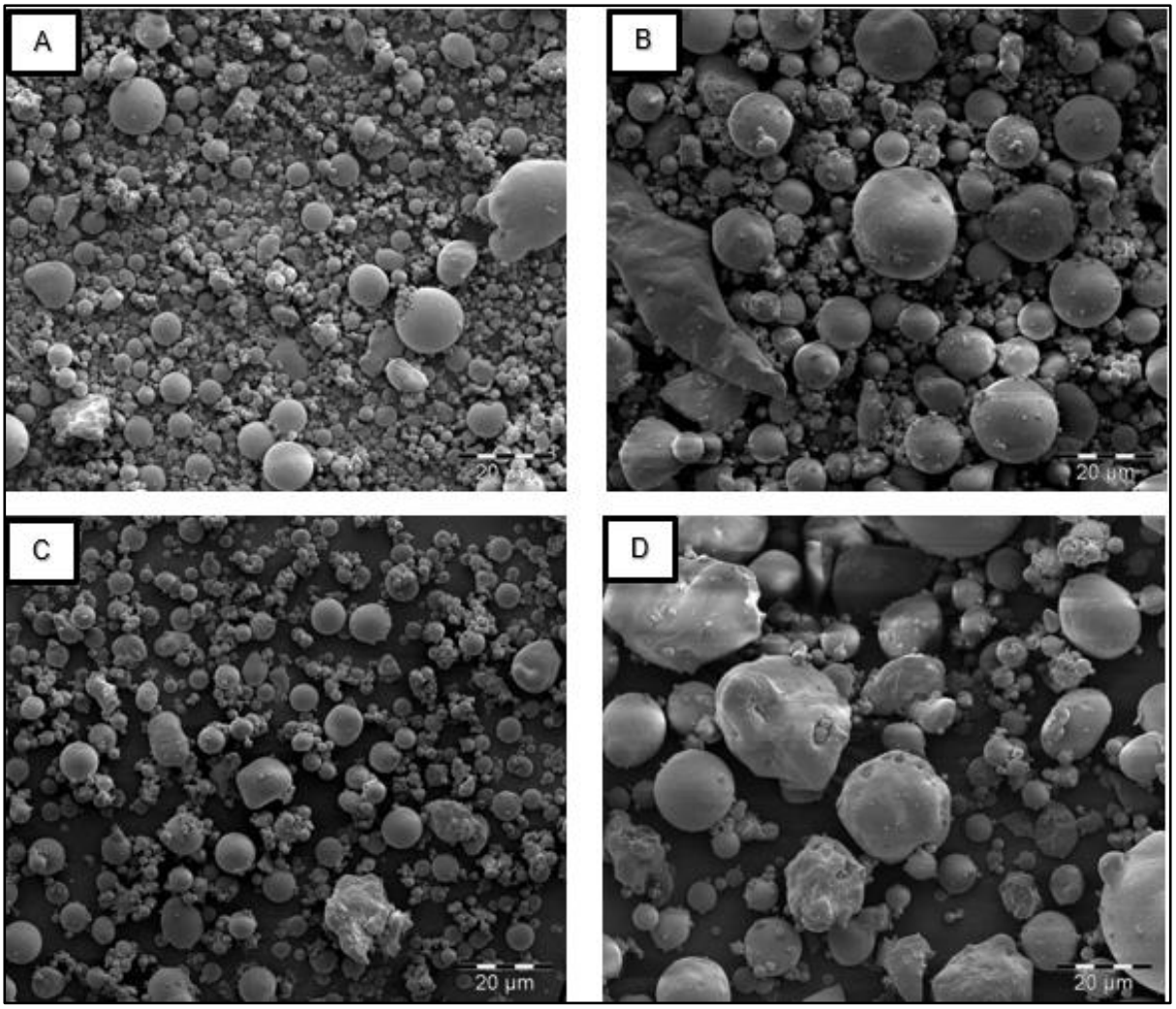

Figure 11: SEM micrographs of A) cyclone ash, B) DuraPozz ash, C) SuperPozz ash, D) SuperPozz Tailings ash.

Particle size analyses were conducted on the four remaining samples at the Chemical Engineering Department of the North West University, Potchefstroom, using the Malvern Mastersizer2000. The particle size distribution is shown by a distribution curve as in Figure 12 through 15. Uniformity in size is shown by a Gaussian distribution as in Figure 14, representing the SuperPozz sample, as to a bimodal distribution shown by the distribution curves of the other samples.

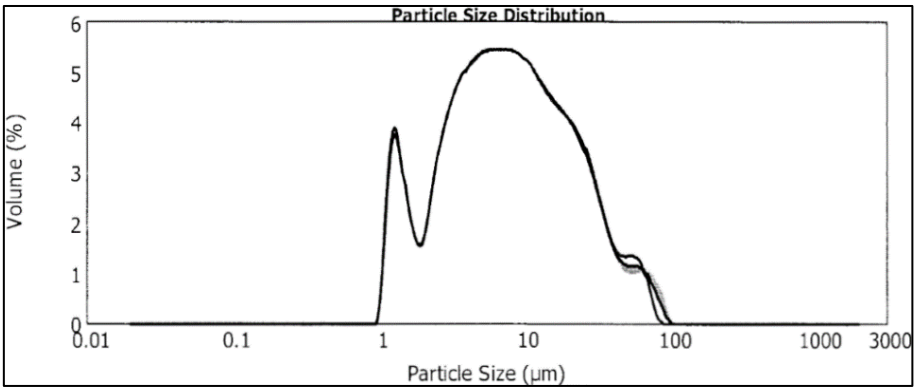

Figure 12: A particle size distribution curve of a Cyclone fly ash sample.

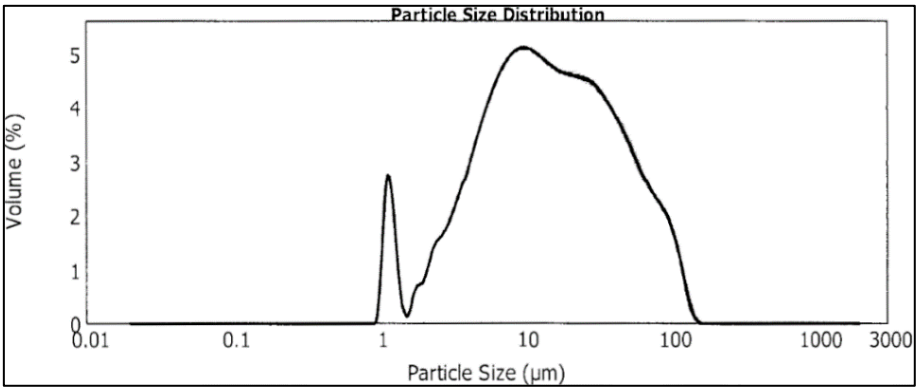

Figure 13: A particle size distribution curve of a DuraPozz fly ash sample.

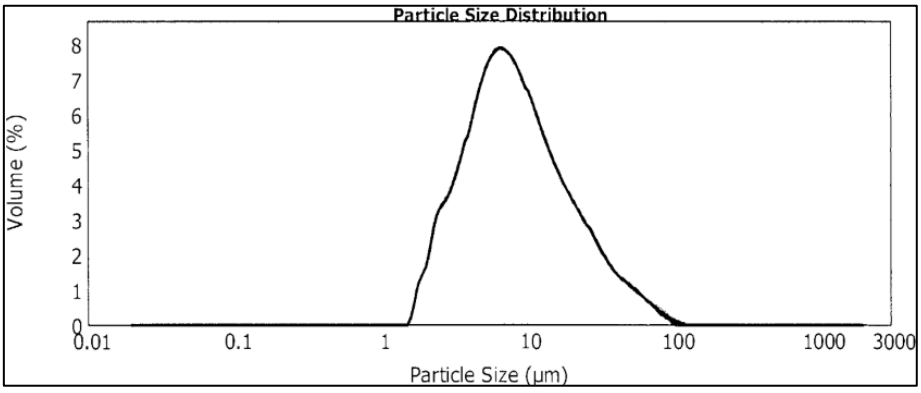

Figure 14: A particle size distribution curve of a SuperPozz fly ash sample.

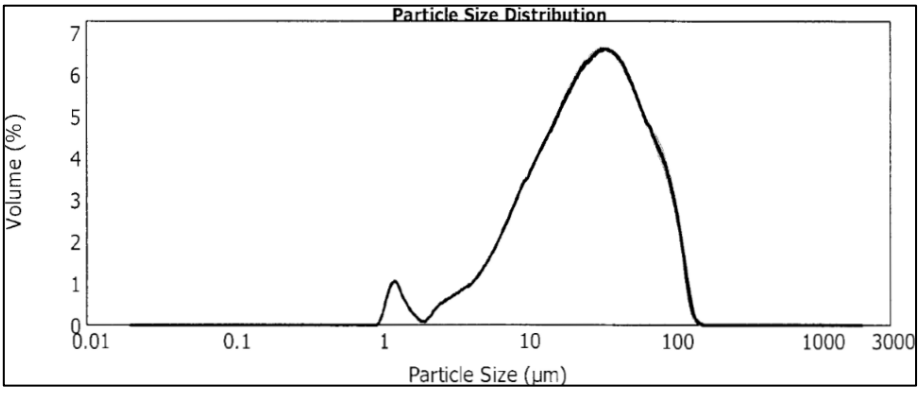

Figure 15: A particle size distribution curve of a SuperPozz Tailings fly ash

An average particle size of 8.0 µm and only 10% of its particles larger than 27.0 µm in diameter implies that, among the four samples, with diameter fractions as compared in Table 4, the SuperPozz sample is sufficiently homogeneous in size in order to achieve uniformity in dispersion and strengthening.

Table 4: A comparison of the size distribution of the particles of the four samples of fly ash considered for reinforcement.

Sample	10% of Sample	50% of Sample	90% of Sample
Cyclone	≤ 1.9 µm	≤ 7.6 µm	≤ 29.5 µm
DuraPozz	≤ 3.3 µm	≤ 14.4 µm	≤ 61.7 µm
SuperPozz	≤ 3.1 µm	≤ 8.0 µm	≤ 27.0 µm
SuperPozz Tailings	≤ 7.0 µm	≤ 27.8 µm	≤ 78.4 µm

From the data, SuperPozz fly ash particles are selected as reinforcing particles, for the manufactured SG42 iron, on the grounds of uniformity in shape and size. Table 5 shows an approximate composition of SuperPozz obtained from Ash Resources (Pty.) Ltd.

Table 5: Approximate oxide analysis of SuperPozz fly ash as provided by Ash Resources (Pty.) Ltd.

SiO_2	Al_2O_3	Fe_2O_3	CaO	Other *
53.5%	34.3%	3.6%	4.4%	4.2%

***** TiO_2, MgO, K_2O, P_2O5, SO_3, SrO, BaO, Na_2O, ZrO_2, Cr_2O_3, and V_2O_5 (A.A. Landman, 2003).

3.3 Compo-casting Setup

Casting were carried out in the foundry of the Materials Research Department at the Council for Scientific and Industrial Research (CSIR) in Pretoria, South Africa. The casting setup inside the foundry is shown in Figure 16.

Figure 16: The casting setup in the foundry at CSIR, Pretoria.

A schematic sectioned view of the compo-casting configuration, with the coil, crucible, and the stirrer is shown in Figure 17.

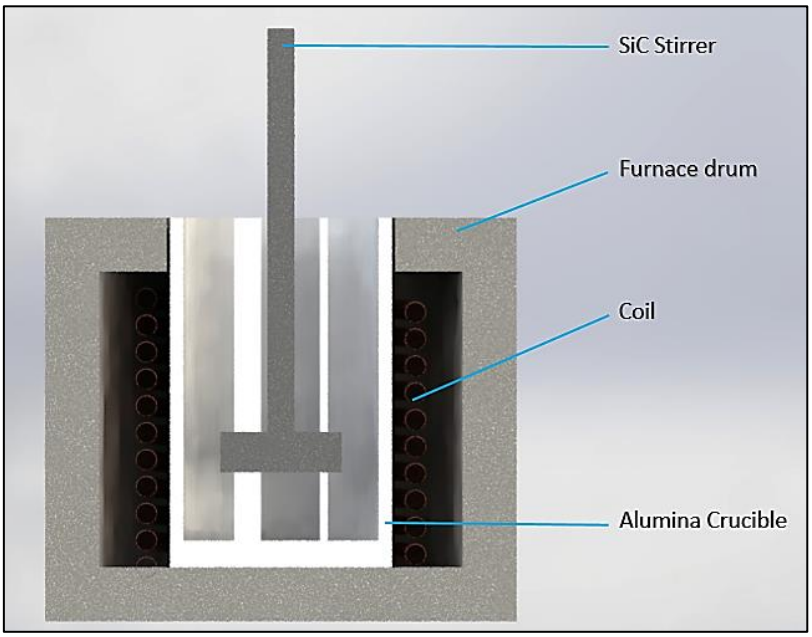

Figure 17: A schematic representation of the compo-casting setup.

3.3.1 Induction Furnace

The VIP POWER-TRAK 200-10 induction furnace was used during the experiment. An alumina crucible was mounted to the furnace shown in Figure 18, using alumina cement, to limit quick expansion due to thermal shock and hence prevent fracture of the crucible. The furnace is allowed to tilt and the crucible is fixed to the furnace for the duration of the experiment. The ability to control the temperature and the open top of the furnace makes the furnace suitable for compo-casting, in that a stirrer can easily be used to stir the melt.

Figure 18: The furnace and power unit of the VIP POWER-TRAK 200-10 induction furnace.

3.3.2 Stirrer

The stirrer that was used for the stirring of the semi-solid melt was a 10mm thick (SiC) plate, cut into a shape, shown in Figure 19, using a diamond cutting wheel. Since an induction furnace heats all electrical conductive materials through induced eddy currents, resulting from electromagnetic induction by the coil, the stirrer material had to be selected from ceramics. SiC is a semi-conductor, known for its application in electrical furnaces as resistance heating elements. As seen in Table 6, a low thermal expansion and a high thermal conductivity, gives SiC sufficient thermal shock resistance, which, together with good mechanical properties and availability resulted in SiC being selected as stirrer material for the purpose of stirring the semi-solid melt in this study.

Table 6: Mechanical and thermal properties of SiC.

Flexural Strength	550 MPa
Fracture Toughness	6.4 MPa-$m^{1/2}$
Maximum use Temperature	1650 °C
Thermal conductivity	120 W/m°K
Coefficient of Thermal Expansion	4.0 x 10^{-6} / °C

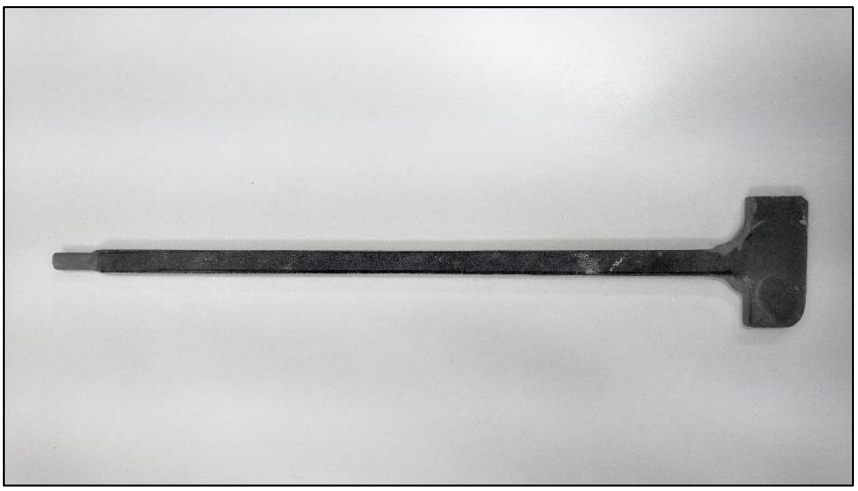

Figure 19: The SiC stirrer, cut from SiC plate, that was used to stir the semi-solid melt in this study.

3.3.3 Ladle

Since the height of the induction furnace compromised the ease and accuracy of casting into a mould, the casting process made use of a ladle, consisting of an alumina crucible, fixed into a steel ladle with alumina cement, to limit sudden expansion and ultimately prevent the fracture of the crucible.

3.4 Compo-casting Procedure

The configuration for compo-casting, in this study made use of the induction furnace, an alumina crucible, and a stirrer. Stirring was applied to the melt in semi-solid state and is operated by a hand-held mechanical motor. The casting procedure consists of three castings of which one is the control and two serve as feasibility experiments.

3.4.1 Trial Casting

Prior to the actual casting procedure, a trial casting was conducted in order to obtain an indication of the viscosity of the melt, at semi-solid temperature, and after reinforcement. The trial concluded that the viscosity at the eutectic temperature, 1150°C, is such that stirring can be conducted, however once reinforcement is added, the temperature had to be increased to increase the fluidity of the melt.

During the trial, 1.5% weight percentage of preheated fly ash particles were added to the melt and resulted in a highly viscous mixture. The low density of the reinforcing particles gave rise to 1.5% being excessive, such that it compromised the stirring. With this percentage of particles in the melt, the required fluidity could only be achieved at a temperature of 1400°C, which is in the pure liquid phase of the melt. For the purpose of this feasibility study, the addition of reinforcing particles was limited to 0.8% weight percentage in order to obtain a stir-able mixture. 0.8% was chosen as the amount of reinforcement, based on the findings on the viscosity of the melt during the trial that was conducted. A percentage below 1% was chosen in order to have an increased fluidity, but still incorporate enough particles to sufficiently test the feasibility of particle reinforcement.

3.4.2 Mould Manufacturing and Casting of the Control Sample

An additive manufactured sand mould, shown in Figure 20, was used to cast the control samples. Manufactured by Vaal University of Technology (VUT), South Africa, the mould consisted of a fine silica sand that was bonded by resin. The mould was made up of two halves and consisted of six tensile specimens and two charpy specimens connected to a runner system.

Prior to melting, casting preparations were done to both, ensure a controlled procedure, and prevent significant temperature fluctuations that might prolong or compromise the casting process. The furnace crucible was preheated to 800°C by placing a steel billet inside to be heated by induction and in turn heat the crucible by radiation. The ladle was preheated with a blow flame to prevent a significant drop in temperature of the melt in the ladle.

For the purpose of a feasibility study, 0.8% weight percentage of fly ash was weighed of for each reinforcing experiment and placed in a muffle furnace at 700°C for 2 hours to reduce the unburned carbon content of the fly ash. Prior to reinforcement, the fly ash and stirrer was preheated to 1000°C in an attempt to prevent a sudden loss in temperature of the melt during reinforcement

The control experiment, shown in Figure 21, consisted of the casting of an unreinforced SG42 iron, with the composition in Table 3. Pig iron and ferrosilicon was placed in the preheated alumina crucible, in the furnace, and melted at 1600°. Once all the contents were in the full liquid phase, the melt was poured into the ladle, containing the nodulising content, while the inoculant was introduced in the pouring stream. After the exothermic flair from the magnesium treatment, the melt, with a temperature of 1120°C, was poured back into the furnace and reheated to 1400°C to achieve sufficient fluidity for casting. The melt was cast into the mould, presented in Figure 20, and left to cool at ambient conditions.

Figure 20: The additive manufactured sand mould, consisting of two halves that are clamped together as in the bottom figure.

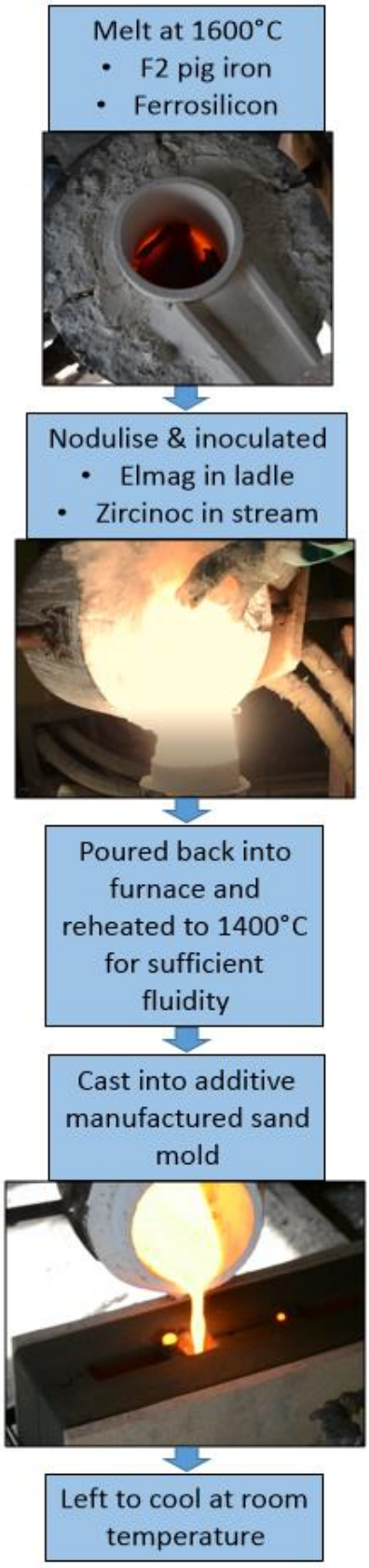

Figure 21: A flow diagram of the casting procedure of the control sample of SG42 in the study.

The microstructure of the control sample, under the polarising microscope exhibited a predominant presence of graphite nodules, as seen in Figure 22, in a magnetic matrix, indicating the presence of ferrite. Smaller nodular precipitates of graphite are visible with higher magnification. There exist small amounts of flake graphite in the structure, attributed to magnesium fade as a result of reheating to a sufficient casting temperature, during which some nodulising magnesium content may have oxidised and floated to the slag of the melt.

Figure 22: A polished and etched surface of the control sample viewed under the polarising microscope at 100X magnification.

A spectrographic analysis was conducted on the control sample, with an optical emission spectrograph while carbon and sulphur was measured by the combustion in oxygen method. As shown in Table 7, the analysis reports C, Mn, S, P, Si, Cr, Mo, Ni, Cu, Al, V, Ti, Mg, Pb, and Sn.

Table 7: The spectrographic composition (wt%) of the control sample.

Element	Control
C	3.650
Mn	0.020
S	0.027
P	0.016
Si	2.380
Cr	0.020
Mo	<0.010
Ni	0.020
Cu	<0.010
Al	0.019
V	<0.005
Pb	<0.005
Sn	<0.005
Ti	<0.005
Mg	0.057

The spectrographic analysis, in Table 7, was compared to the desired SG42 analysis in Table 1, in order to assess the differences in relevant elements in the composition and make changes to the charge analysis in Table 3; however, the compositions of the desired and obtained SG42 iron correlated sufficiently and no changes was necessary.

Table 8: A comparison in composition (wt%) between the desired SG42 and the control sample of this study.

Sample	C%	Si%	Mn%	P%	Mg%	S%	Fe%
Desired SG42	3.1 – 3.8	2.2 – 2.7	0.15 – 0.3	0.04 Max	0.02 - 0.05	0.02 Max	Balance
Control	3.6	2.4	0.02	0.02	0.06	0.03	± 93.8

From the resulting microstructure in Figure 22, and the spectrographic composition, in Table 7, it was noted that magnesium fade had occurred to an extent that allowed the formation of graphite flakes, instead of nodules. Reheating after magnesium treatment caused a reduction in both carbon and magnesium content in the melt. For further experimental control, and to attempt to increase the recovery of magnesium, two different processing methods were applied during the casting of reinforced samples. Casting Method 1 (CM1), presented in 3.4.3 below, consisted of a similar casting procedure as that of the control sample, and Casting Method 2 (CM2), presented

in 3.4.4 below, saw magnesium treatment being done just prior to casting in order to achieve an increased recovery of magnesium.

Further, during the casting of the control sample, in the sand mould in Figure 20, it was observed that a decrease in the fluidity of the melt would cause cold shut during casting, as the cast tree of the mould consisted of small passages that might obstruct the flow of the semi-solid melt during the compo-casting methods. As alternative, a simplified shape was machined from alumina (Al_2O_3) fibre, as shown in Figure 23, in order to allow the semi-solid, reinforced melt to be cast without obstruction.

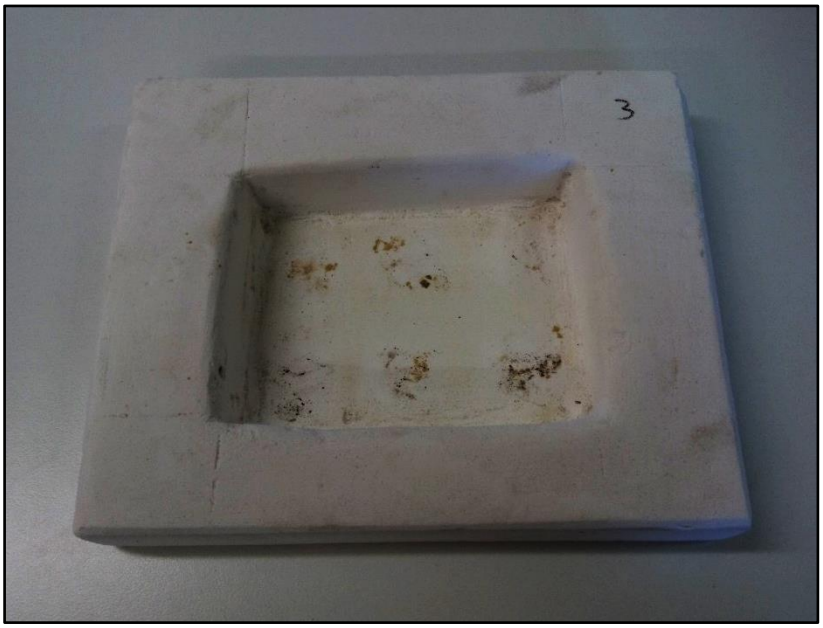

Figure 23: A simplified shape, machined from alumina fibre, used as a mould in the casting of the reinforced SG42.

3.4.3 Casting Method 1 (CM1)

The first reinforcing method consisted of the introduction of fly ash particles into ductile iron through the method of compo-casting. Pig iron and ferrosilicon was placed in the preheated alumina crucible, in the furnace, and melted at 1600°C. Once all the contents were in a full liquid state, the melt was poured into the ladle, containing the nodulising content, while the inoculant was introduced in the pouring stream. After the exothermic flair, the melt, was poured back into the induction furnace and the temperature was reduced and maintained at just above the eutectic temperature, 1150°C, to obtain a thixotropic consistency of the melt. The temperature was

checked frequently by placing a thermocouple in the melt to ensure that the temperatures of the melt and the furnace were the same.

With the melt at 1150°C, stirring was initiated at 400 rpm and preheated fly ash particles were steadily introduced into the melt from a crucible, whilst stirring was maintained. The temperature was checked frequently by placing a thermocouple in the melt. The temperature of the melt was slightly increased throughout the process to maintain the thixotropic consistency of the melt. The stirring and addition of particles were limited to one minute in order to limit the loss of the nodulising Mg content in the melt. After stirring was completed, the mixture was cast into the alumina mould, shown in Figure 23 and 24, in semisolid state at a temperature of 1200°C. After the melt was cast into the mould, the casting was left to cool at ambient conditions.

3.4.4 Casting Method 2 (CM2)

The second reinforcing method also consisted of the introduction of fly ash particles into ductile iron through the method of compo-casting. Pig iron and ferrosilicon was placed in the preheated alumina crucible, in the furnace, and melted at 1600°C. Once all the contents were in a full liquid state, the temperature of the melt was decreased to, just above 1150°C, the eutectic temperature. The temperature was checked frequently by placing a thermocouple in the melt to assure the temperatures of the melt and furnace are the same. With the melt at 1150°C, stirring was initiated at 400 rpm and preheated fly ash particles were steadily introduced into the melt from a crucible, whilst stirring was maintained. The temperature was checked frequently by placing a thermocouple in the melt. The temperature of the melt was slightly increased throughout the process to maintain the thixotropic consistency of the melt. After stirring was completed, the melt, at 1250°C, was poured into the ladle, containing the nodulising content, while the inoculant was introduced in the pouring stream. After the exothermic flair, the melt temperature was measured at 1320°C, and was cast into the alumina mould, shown in Figure 23 and 24, where after the casting was left to cool at ambient conditions.

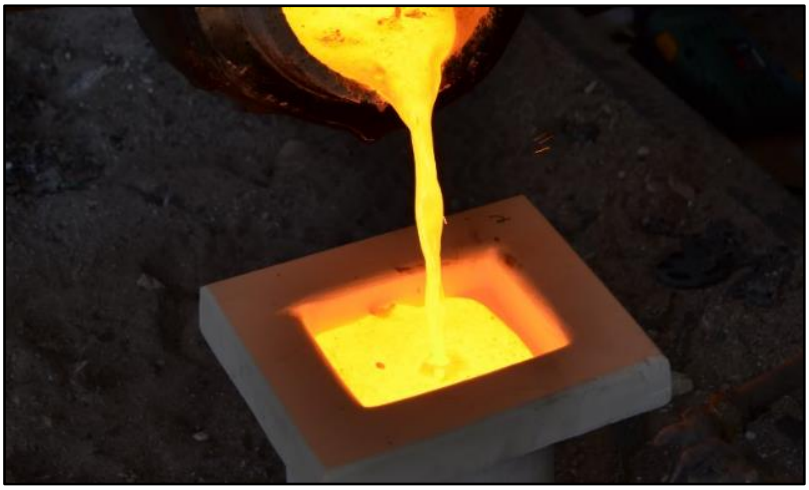

Figure 24: The semi-solid melt being cast into an alumina mould. (Casting Methods 1 & 2)

3.5 Preparation and Examination of Test Specimens

3.5.1 Specimen Preparation

After solidification and cooling, the castings were removed from the mould where after samples from each casting were mounted, polished and etched, using a 2% concentrated Nital etchant, consisting of nitric acid and ethanol. Tensile specimens, shown in Figure 26, were machined from the control casting, as well as from CM1 and CM2, adhering to standard specimen dimensions (ASTM, 2010). The surfaces of all specimens were polished after machining to reduce the probability of fracture as a result of a stress concentration around machining grooves.

Charpy specimens, shown in Figure 27, were also manufactured from the control casting, as well as CM1 and CM2, with a 2mm deep V-notch. As a result of porosity, in CM1 and CM2, and more shrinkage than expected, especially in the case of CM1, charpy specimens were smaller than the standard 10mm x 10mm x 55mm and less than the conventional (three) charpy specimens could be manufactured, from each casting, for testing. For this reason, impact tests were only conducted for the purpose of comparison between the control, CM1, and CM2.

The different sections of the castings, from which tensile and charpy specimens were machined are indicated in Figure 25. Tensile specimens 1 and 4 were cut from the sides of each casting, while tensile specimens 2 and 3 were cut from the middle sections of the castings. The specimens were numbered in order to observe the difference in tensile strengths in specimens with different microstructural characteristics due to different cooling rates.

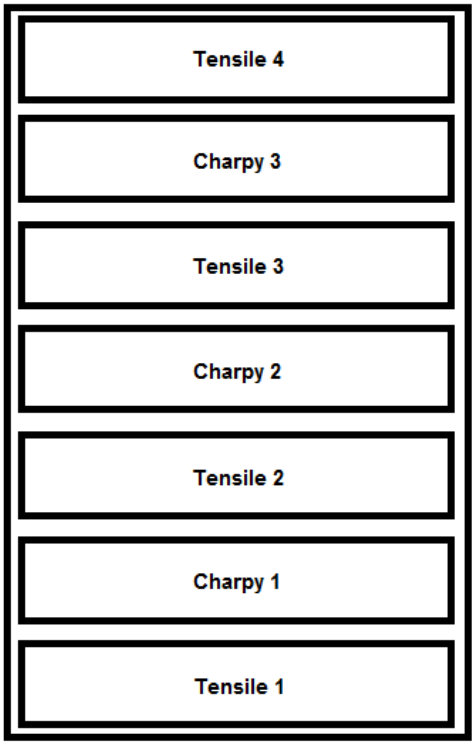

Figure 25: A representation of the simplified shape alumina mould, indicating the locations of the specimens in the mould.

Figure 26: A machined and polished tensile specimen after ASTM standard: A 536 – 84.

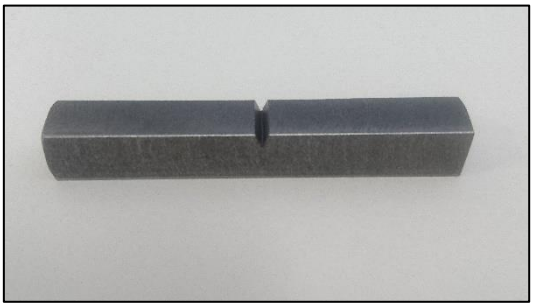

Figure 27: A charpy V-notch specimen manufactured from the castings, after ASTM standard: E26-16a.

3.5.2 Microstructure Examination

A microstructure examination of each sample was conducted to determine the shape of the graphite precipitates and to scan for any visible inclusions. A 100X enlargement was used for the examination of the microstructure. Afterward, fracture surfaces of tensile specimens were examined using SEM, in order to scan for visible inclusions and obtain a point analysis of any impurities with characteristics of fly ash particles.

3.5.3 Spectrographic Analysis

A sample of each casting was sent for cast iron spectrographic analysis at Scrooby's Laboratory Service, in Benoni, South Africa. The analysis was done with an optical emission spectrograph while carbon and sulphur was measured by the combustion in oxygen method. The analysis reports C, Mn, S, P, Si, Cr, Mo, Ni, Cu, Al, V, Ti, Mg, Pb, and Sn.

3.5.4 Tensile Tests

Tensile tests were conducted at room temperature using the MTS landmark testing station, installed in the Mechanical Laboratory of the Mechanical Engineering Department of the North West University, Potchefstroom, South Africa. The standard crosshead speed control method (ASTM, 2010) was used during tensile testing, adhering to ASTM standard E8/E8M – 09, of which the crosshead speed is calculated as:

$$Crosshead\ speed\ =\ guage\ length\ \times 0.015\ \pm 0.003\frac{mm}{mm}/min$$

$$Crosshead\ speed\ = 32mm \times\ \pm 0.003\frac{mm}{mm}/min$$

$$Crosshead\ speed\ = 0.48\ mm/min$$

The tensile specimens were clamped in the crossheads at a pressure of 15MPa where after a constant crosshead separation speed was applied, as calculated above.

Figure 28: The crosshead clamps of the MTS landmark testing station shown with a fractured tensile specimen after testing.

3.5.5 Charpy Test

Standard charpy impact tests were conducted on V-notched bars, adhering to ASTM standard E26-16a. Tests were conducted using the SCHENCK TREBEL pendulum impact testing aparatus.

Chapter 4

Results and Discussion

In this chapter the results obtained from the spectrographic analyses, microstructure examinations, and mechanical testing conducted in chapter 3, are presented and discussed.

4.1 Spectrographic Analyses

The spectrographic analysis conducted on the specimens from the control, CM1, and CM2 reported the compositions as in Table 9.

Table 9: Spectrographic analyses results.

Element	Control	CM1	CM2
C%	3.7	3.4	4.2
Mn%	0.02	0.02	<0.01
S%	0.03	0.01	0.02
P%	0.02	0.03	0.05
Si%	2.4	2.4	1.9
Cr%	0.02	0.03	0.02
Mo%	<0.01	<0.01	0.05
Ni%	0.02	0.02	0.02
Cu%	<0.01	<0.01	<0.01
Al%	0.02	0.01	0.02
V%	<0.005	0.02	<0.005
Pb%	<0.005	<0.005	0.05
Sn%	<0.005	<0.005	0.08
Ti%	<0.005	0.01	<0.005
Mg%	0.06	0.01	0.1

The analyses reveal a significant difference in the carbon content between the samples. Since the pig iron is the only charge material that contains carbon, it is clear from the control and CM1 in Table 9 that longer processing times of the melts decreased the carbon content significantly. The addition of fly ash can result in an increase the carbon content of the iron, due to unburned carbon in the ash, as can be the case in CM2. The different processing routes followed for the manufacturing of CM1 and CM2 caused CM1 to be exposed to high temperatures for longer. The control and CM1 was exposed to heat from the furnace during the initial melt and after magnesium treatment, whereas CM2 was only exposed to the furnace heat once during the initial melt. This

led to a fade in the initial carbon content, and that which might have been added, as unburned carbon, through the fly ash. The same can be said for the magnesium content, which oxidises at melting temperatures, causing a decrease in the total magnesium content in the melt. There is however a higher Mg content in the CM2 sample, as can be seen in microstructure examination, in Figure 30, where graphite precipitates had a much more spheroidised shape compared to the other samples.

4.2 Microstructural Examinations

The microstructure of a sample from CM1, shown in Figure 29, exhibited a very fine flake graphite structure. The microstructure revealed a negligible presence of nodular graphite, indicating that the nodulising magnesium content faded during stirring at semi-solid temperature. Indicated in Figure 29 are dendrites that are typical of austenite, in that austenite coring is visible in the microstructure, together with inter-dendritic carbides. This indicates high degrees of undercooling, which serves as an explanation for the fine flake graphite, known as undercooled graphite. The microstructure, even at higher magnification, do not reveal any visible irregularities, impurities or particles with characteristics of fly ash.

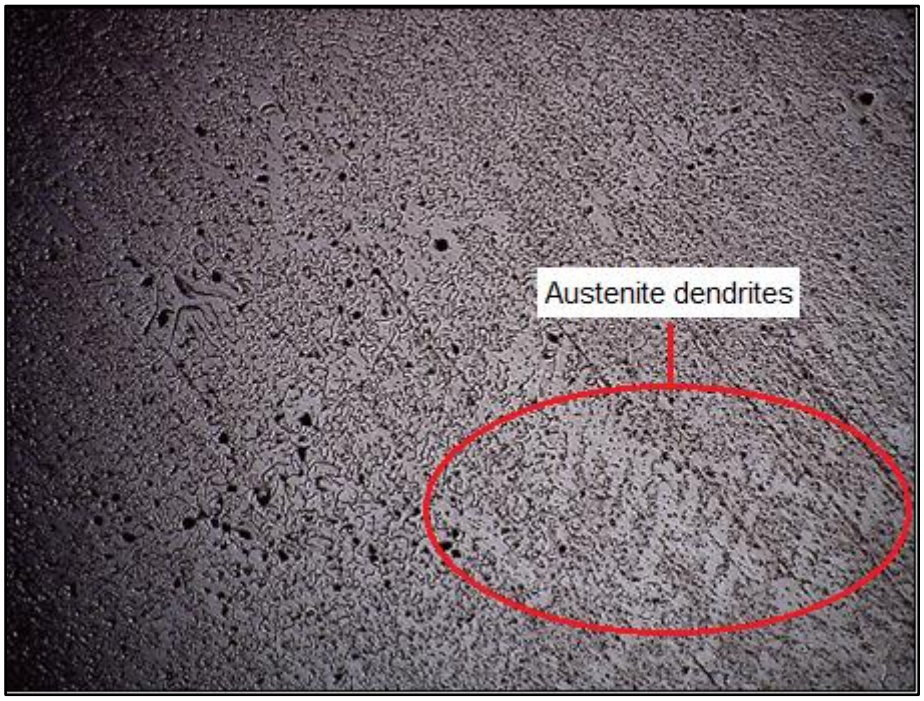

Figure 29: An etched sample of CM1, viewed under the polarising microscope at 100X magnification.

The microstructure of a sample from CM2 under the polarising microscope exhibited a well distributed nodular graphite structure in a magnetic matrix, mostly made up of ferrite. The microstructure revealed no flake graphite, indicating that magnesium treatment just prior to casting resulted in a higher recovery of the nodulising magnesium content. The microstructure does not reveal any visible irregularities, impurities or particles with characteristics of fly ash.

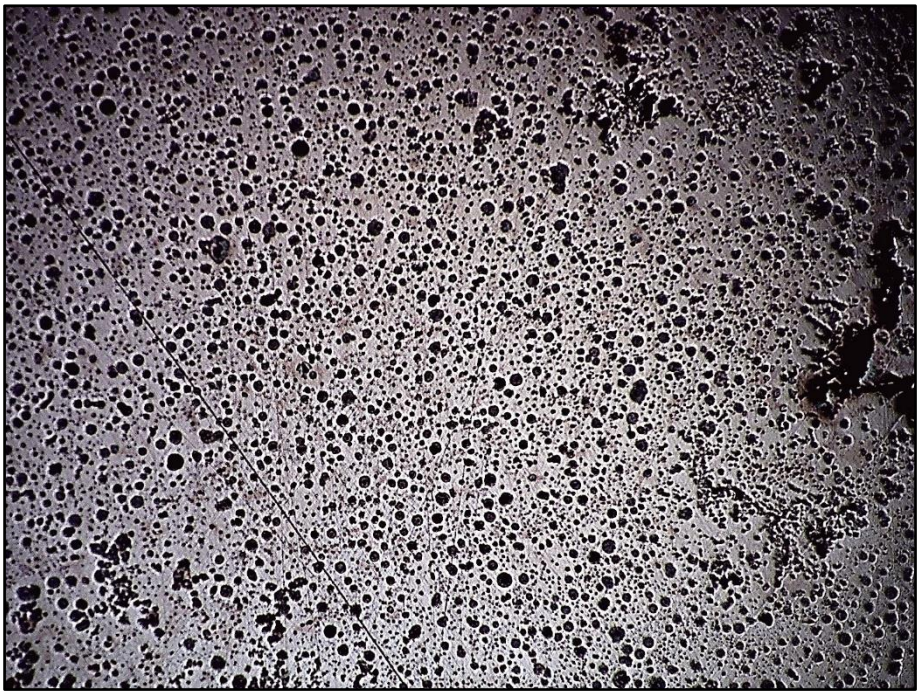

Figure 30: An etched sample of CM2, viewed under the polarising microscope at 100X magnification.

The fracture surfaces of the tensile specimens from the control, CM1, and CM2 were examined under a scanning electron microscope to determine the mode of fracture and whether any fly ash particles are visible in the fracture surface.

Upon good nodularity and distribution of graphite, relatively ductile fracture surfaces were exhibited by the control sample. This was revealed by dimples in the fracture surface, shown in Figure 31 and 32. Dimples are caused by cavities that result from inclusions or coarser precipitates, such as graphite. During tension the material between the cavities yield and is “necked and sheared” to create dimples (M. Möser). The fracture surfaces also exhibit dimples with lost graphite nodules, in cases where graphite nodules became loose from the matrix during fracture.

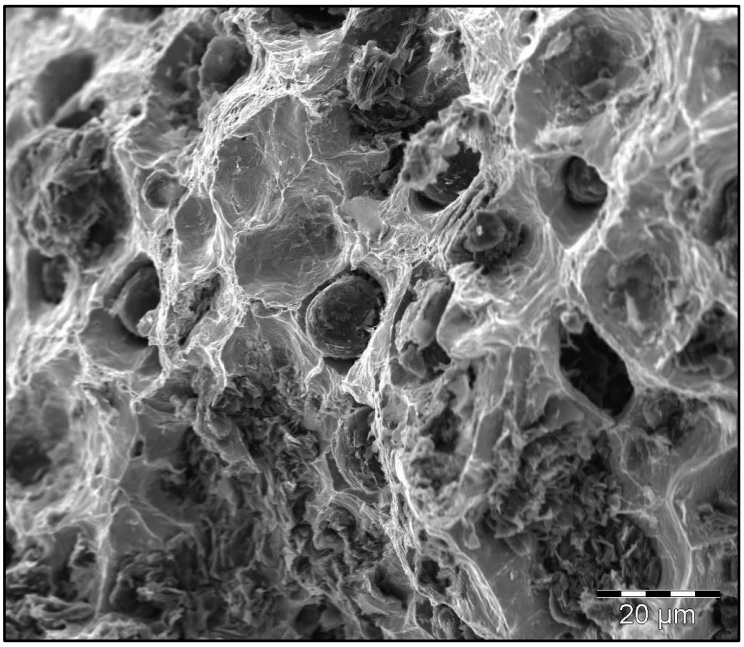

Figure 31: A micrograph of the fracture surface of the control sample, exhibiting sites of lost graphite nodules.

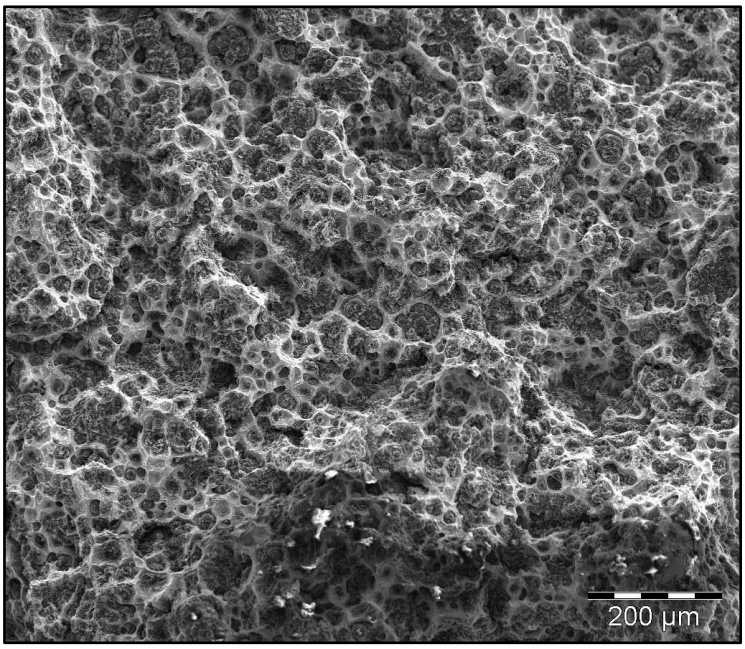

Figure 32: A micrograph of the fracture surface of the control sample, displaying dimples, indicating ductile fracture.

For CM1 the fracture surface is purely brittle and displays only fracture along graphite flakes, as seen in Figure 33. The fracture surface exhibited no visible fly ash particles during the examination.

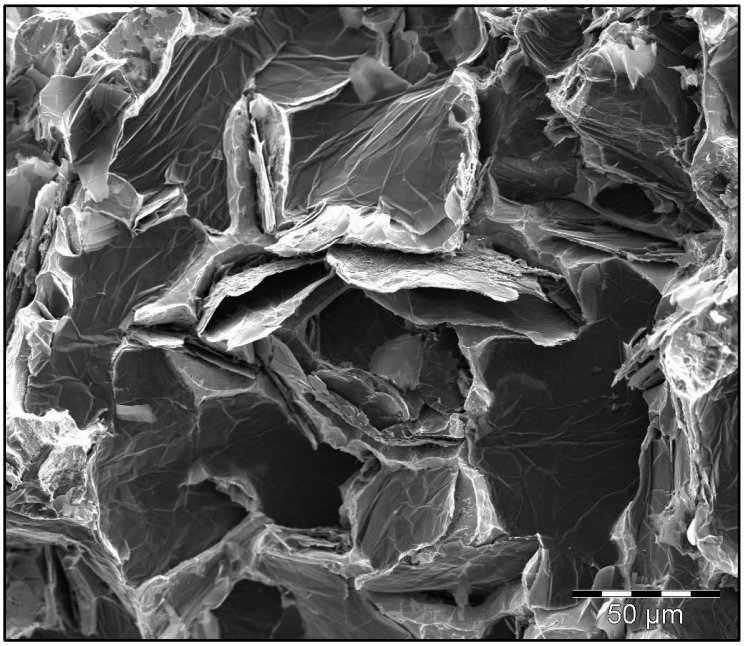

Figure 33: A micrograph of the fracture surface of a sample from CM1, indicating brittle fracture along graphite flakes.

The fracture surface of a sample of CM2 revealed a ductile fracture surface, indicated by dimples. Good nodularity, together with a good distribution of graphite is observed. The fracture surfaces have in some cases displayed impurities, that have been analysed by SEM, shown in Figure 34, and found to be partially unreacted lumps of magnesium in the matrix.

Further examination of the fracture surface led to the discovery of foreign spherical particles in the matrix, that were analysed by point analysis, and captured in Table 10, and recorded high scores of CaO, known to be a major content (Medhat H. Shehata and Michael D.A. Thomas, 2000) of SuperPozz fly ash. The particles, however, do not seem to be bonded to the matrix material and merely act as loose inclusions that were trapped during solidification.

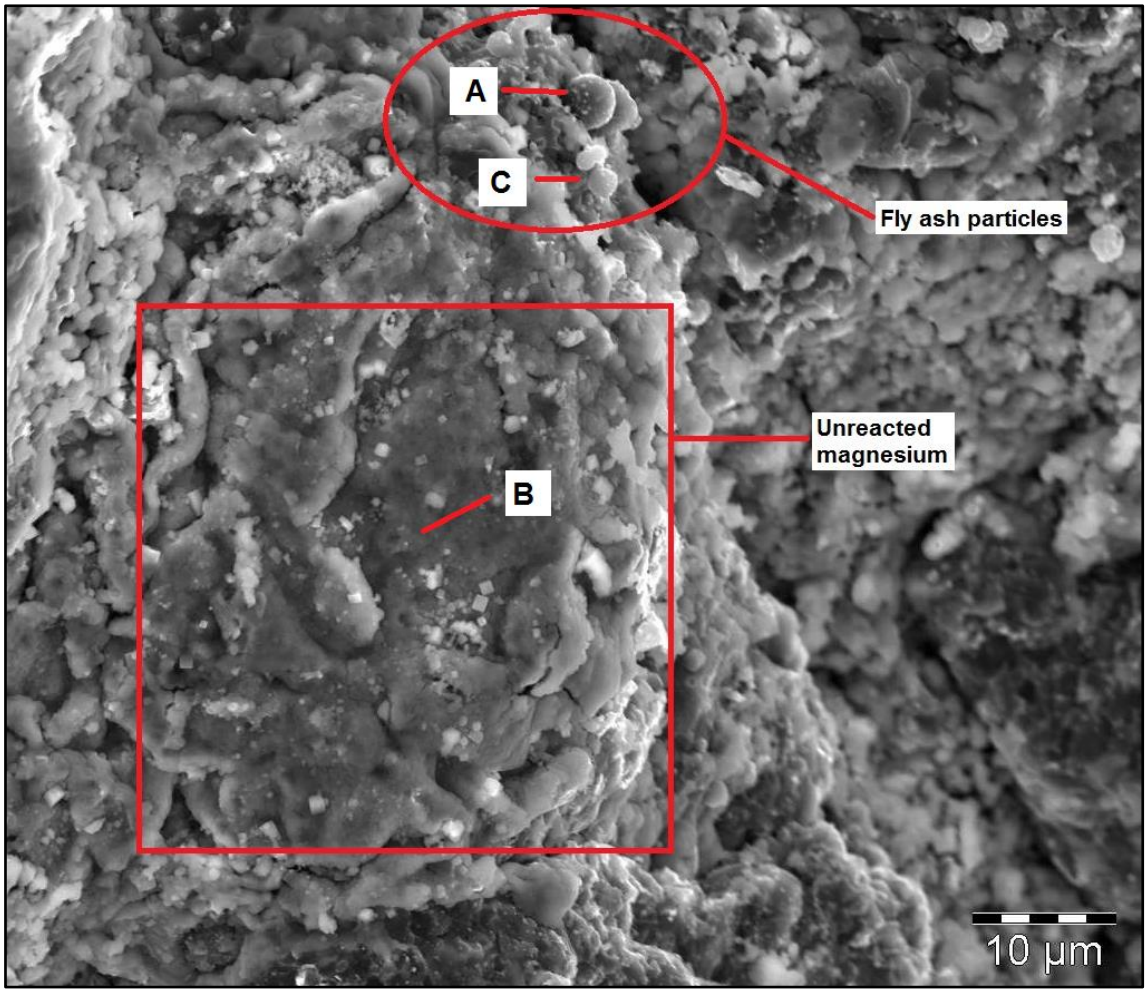

Figure 34: A micrograph of the fracture surface of a sample from CM2 displaying sites A, B, and C on which point analyses were taken, showing unreacted magnesium and fly ash particles.

Table 10: Compositions obtained from point analyses of sites identified in Figure 34.

Sites	C	O	Mg	Si	S	Ca	Fe	Total
A	59.49%	10.07%	0.36%	0.4%	0.15%	**16.96%**	12.57%	100
B	8.41%	29.05%	**9.72%**	1.43%	0%	12.27%	39.11%	100
C	90.81%	3.26%	0.31%	0.37%	0%	0.71%	4.55%	100

No traces of Ca are reported in the analysis, despite the presence of CaO particles on the fracture surface in Figure 34; this is explained by the area specific nature of spectrographic analyses, during which only certain areas of the casting was analysed. The Al, Si, and S contents is lower in sample CM2 than in the control sample, thus, dismissing the possibility of the presence of fly ash in these specific sites of the sample.

The possibility of compounds or impurities in the fly ash dissolving in the matrix cannot be ignored, however with fly ash, in this case, only being 0.8% of the total weight of the melt, significant increases in any element in a reinforced sample cannot necessarily be attributed to the presence of fly ash.

4.3 Mechanical Testing Results

4.3.1 Tensile Tests Results

The results obtained from tensile testing on specimens from the control casting, and the two casting procedures are shown in Table 11.

Table 11: Tensile test results

Specimens		Ultimate Tensile Strength (MPa)	Average (MPa)
Control	1	404.4	405.3
	2	**408.1**	
	3	401.7	
	4	407.0	
CM1	1	144.9	173.2
	2	180.5	
	3	178.3	
	4	**189.1**	
CM2	1	**446.4**	377.2
	2	361.2	
	3	324.6	
	4	376.7	

From the results in Table 11, the maximum tensile strength obtained from each casting is in bold print. It is clear that the average tensile strength decreased in both attempts to reinforce the ductile iron. CM1 experienced the largest decrease, which is attributed to significant magnesium fade during the procedure, resulting in a grey iron. When compared to conventional grey irons, the composition is similar to that of an ASTM A48 grey iron, apart from the 0.2% shortfall in Mn content of CM1. In such a case, an increase in tensile strength from 130MPa to 170MPa is observed in the grey cast iron with the addition of fly ash.

CM2 yielded a significantly higher tensile strength, however still lower than that of the control. Specimen 1 from this procedure is an outlier with an UTS of 446.4 MPa. The fracture surface of this specimen was examined using the SEM and found that uniformity in size and distribution of graphite in the fracture surface, shown in Figure 35, and the near absence of impurities likely

resulted in a tensile strength higher than that of the control. However, one cannot draw a conclusion as to the presence of fly ash, since the fracture surface is considered to be the weakest point in the specimen; the possibility of strengthening in the rest of the specimen can thus not be ruled out.

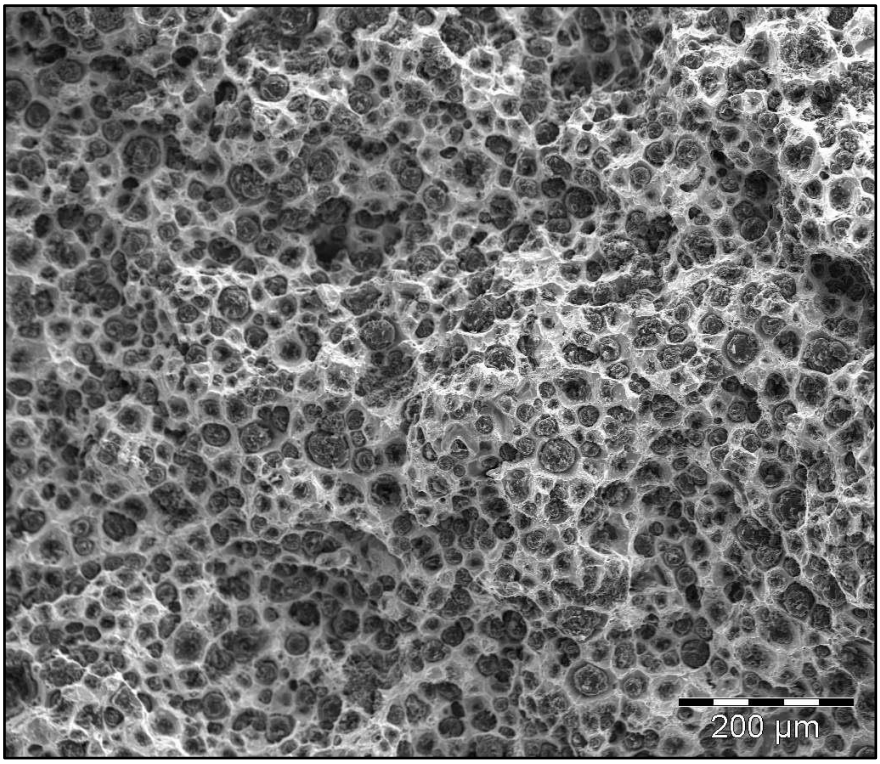

Figure 35: A micrograph of the fracture surface of specimen 1 from CM2, showing uniformity in size and distribution of graphite.

4.3.2 Impact Test Results

The porosity of the reinforced castings, shown in Figure 36, compromised the machining of test specimens, during which only one successful charpy specimen could be manufactured from each of the two castings from the reinforcing methods. Specimens that were machined contained large cavities on the surface and likely inside the specimens, as a result of insufficient fluidity in semi-solid casting. The results obtained from impact testing on charpy V-notch specimens are shown in Table 12.

Figure 36: An offcut from CM2 exhibiting high levels of porosity.

Table 12: Impact test results.

Specimen	Average energy absorbed (J/m^2)
Control	89871.7
CM1	42548.7
CM2	89049.5

The impact test results show a correlation between the impact strength of the control and CM2, where the impact strength of a sample from CM2 is moderately lower than that of the control. The fracture surfaces of the specimens show no significant difference as all specimens display brittle fracture.

Despite the porosity of the castings, the energy absorbed by the second sample serves as proof that in a case of no porosity, the impact strength is not significantly affected by the introduction of fly ash particles as reinforcement.

Chapter 5

Conclusion and Recommendations

4.4 Conclusion

This research proved that the reinforcement of ductile iron with fly ash particles, through the method of compo-casting, in an induction furnace is possible but not likely to be feasible in a non-experimental, uncontrolled environment.

The results obtained from microscopic examination, spectrographic analysis, and mechanical testing indicate that:

i. longer processing times resulted in a loss of elements, necessary to produce a ductile iron, such as carbon and magnesium

ii. magnesium had not fully reacted with the melt in semi-solid phase, in a case of quicker processing

iii. the addition of fly ash brought about negligible changes in the spectrographic composition of the ductile iron

iv. the ductile iron matrix does not seem to sufficiently wet the surface of fly ash particles through the application of compo-casting

v. the impact strength of ductile iron decreases with the addition of fly ash through the process of compo-casting

vi. the tensile strength of ductile iron decreases with the addition of fly ash through the process of compo-casting.

The increased porosity of semi-solid processed metals is confirmed for ductile iron, and in this regard agrees to the findings of H. KHOSRAVI *et al*. (2013) on semi-solid processed aluminium. From the study and above mentioned results the following conclusions can be made:

i. The method of compo-casting, applied to ductile iron, is labour-intensive and subject to precarious results, especially when integrated with conventional casting methods. Longer processing times and an increase in reaction time of magnesium with the melt requires one to account for losses of especially carbon and magnesium during stirring.

ii. Due to a significant increase in viscosity, defect free thin walled castings, such as gate valve housings, are not achievable through conventional casting methods in the casting of ductile iron, in semi-solid phase, with added fly ash particles.

iii. Varying compositions of fly ash can result in varying properties of the iron, since some compounds of fly ash can dissolve in the matrix, due to high processing temperatures, and give rise to different compositions.

iv. Since the ductile iron matrix do not wet the surface of fly ash particles, the necessary strengthening mechanism cannot be achieved through compo-casting. The improvement of the structural strength of a ductile iron is thus not achievable through fly ash reinforcement done through compo-casting, using an induction furnace.

4.5 Recommendations for Further Studies

In the 21st century, cast iron is not a frequent topic for research, however the economic advantages introduce a platform for research into improved mechanical properties of cast iron and thus reduced weight of castings, since ductile iron is still preferred in some critical industrial applications.

Although the incorporation and especially the wetting of fly ash was not sufficiently achieved in this study, the following recommendations can be made for further studies:

i. Larger scale production of fly ash reinforced ductile iron together with broader availability of ceramics, suitable to be used as stirrers, will simplify the process and thus increase the probability to achieve wetting through compo-casting. The volatile nature of a small-scale experiment, especially its susceptibility to temperature changes makes it critical to preheat all equipment and the fly ash prior to the experiment. The preheating of fly ash above 700°C often leads to sintering and clumping of fly ash particles.

   Silicon carbide is a good choice of material for the stirrer, since its resistance to thermal shock is sufficient, however, its increased brittleness after the exposure to high temperatures compromises stirring in a viscous melt at the eutectic temperature of ductile iron. A broader selection of non-conductive materials, such as silicon nitride, should provide sufficient thermal and mechanical properties to serve as stirrer material.

ii. Incorporation of fly ash particles in a ductile iron melt is more probable with magnesium treatment being done after particle addition and stirring. In such a case, surface modification of fly ash is a viable option to promote wetting.

iii. Particle reinforcement of ductile iron is a relatively unexplored field of study of which little documented proof exists. Different casting methods can be attempted to increase wetting, after stirring, such as pressure casting, which have been successful in fly ash reinforced aluminium castings.

iv. Since grey iron is a less complex cast iron, not as susceptible to the fading of elements, it should be easier to process, monitor, and account for losses, in especially carbon, during melting. Achieving strengthening in a cast iron through the addition of fly ash particles seem less precarious with the use of grey iron.

References

ABHIJIT DEY & KRISHNA MURARI PANDEY. 2015. *CHARACTERIZATION OF FLY ASH AND ITS REINFORCEMENT EFFECT ON METAL MATRIX COMPOSITES: A REVIEW.* Review, Department of mechanical engineering, National institute of technology.

AMERICAN MATERIALS SOCIETY 2008. Austenitic Stainless Steels. *Stainless Steels for Design Engineers.* ASM International,.

AMERICAN SOCIETY FOR MATERIALS ASM Metals Hand Book - Properties and Selection Irons, Steels, and High Performance Alloys. 1.

AMERICAN SOCIETY FOR MATERIALS 1996. *ASM Specialty Handbook Cast Irons*, ASM International.

ASTM 2010. Standard Test Methods for Tension Testing of Metallic Materials. *Designation: E8/E8M – 09.* West Conshohocken Pennsylvania ASTM.

DAVIES, J. T. South African Foundry Industry. 2nd VAMCOSA foundries workshop, 2015.

DUCTILE IRON SOCIETY 1998. Ductile Iron Data for Engineers.

FRANCK A GIROT, A. P. M., TSU WEI CHOU Metal Matrix Composites.

G. CHADWICK, L. F. *Metal Matrix Composites - Interfacial phenomena in the solidification processing of Metal Matrix Composites*.

H. J. GRABKE, D. MOSZYNSKI, E. M. MÜLLER-LORENZ & SCHNEIDER, A. 2002. Role of sulphur in carburization, carbide formation and metal dusting of iron. *Surface Interface Analysis,* 34**,** 5.

HASHIM, J., LOONEY, L. & HASHMI, M. S. J. 1999. Metal matrix composites: production by the stir casting method. *Journal of Materials Processing Technology,* 92**,** 1-7.

HIGGINS, R. A. 1993. *Engineering Metallurgy* Great Britain Edward Arnold.

IBRAHIM, I. A., MOHAMED, F. A. & LAVERNIA, E. J. 1991. Particulate reinforced metal matrix composites - a review. *Journal of materials science,* 26**,** 1-2.

K.V. MAHENDRA & K. RADAKRISHNA 2007. Fabrication of Al–4.5% Cu alloy with fly ash metal atrix composites and its characterisation. *Materials Science-Poland,* 25.

KAILAS, P. S. V. Material Science - Dislocations and Strengthening Mechanisms. Bangalore India: Indian Institute of Science.

KAINER, K. U. 2006. Basics of Metal Matrix Composites. *In:* KAINER, K. U. (ed.) *Metal Matrix Composites. Custom Made Materials for Automotive and Aerospace Engineering.* Weinheim: Wiley.

KHOSRAVI, H., BAKHSHI, H. & SALAHINEJAD, E. 2013. Effects of compocasting process parameters on microstructural characteristics and tensile properties of A356−SiCp composites *Transactions of Nonferrous Metals Society China,* 24**,** 2482−2488

KOK, M. 2005. Production and mechanical properties of Al2O3 particle-reinforced 2024 aluminium alloy composites. *Journal of Materials Processing Technology,* 161**,** 6.

LANDMAN, A. A. 2003. *Aspects of solid-state chemistry of fly ash and ultramarine pigments* University of Pretoria.

MEDHAT H. SHEHATA & MICHAEL D.A. THOMAS 2000. The effect of fly ash composition on the expansion of concrete due to alkali-silica reaction. *Cement and Concrete research,* 30**,** 9.

MILEIKO, S. T. *Metal and Ceramic Based Composites,* Chernogolovka Moscow district, 142432, Russia.

MÖSER, M. Fractography with the SEM. *In:* LOUW, S. (ed.) *Fractography with the SEM.*

RAJAN, T. P. D., PILLAI, R. M., PAI, B. C., SATYANARAYANA, K. G. & ROHATGI, P. K. 2007. Fabrication and characterisation of Al–7Si–0.35Mg/fly ash metal matrix composites processed by different stir casting routes. *Composites Science and Technology,* 67**,** 3369-3377.

RAJESHKUMAR GANGARAM BHANDARE & SONAWANE, P. M. 2013. Preparation of Aluminium Matrix Composite by Using Stir Casting Method. *International Journal of Engineering and Advanced Technology,* 3.
RAMACHANDRA, M. & RADHAKRISHNA, K. 2005. the effect of fly ash reinforcement on density, hardness, micro hardness, ductility and ultimate tensile Strength of Al-Si (12%) metal matrix composite. *Journal of Materials Science,* 40.
RAMACHANDRA, M. & RADHAKRISHNA, K. 2007. Effect of reinforcement of flyash on sliding wear, slurry erosive wear and corrosive behavior of aluminium matrix composite. *Wear,* 262**,** 1450-1462.
REDDY, A. C. 1998. Local Stress Differential for Particulate Fracture in AA2024/Titanium Carbide Nanoparticulate Metal Matrix Composites. *National Conference on Materials and Manufacturing Processes.* Hyderabad, Andhra Pradesh, India: Department of Mechanical Engineering, MJ College of Engineering and Technology, Hyderabad, India.
S. AMIRKHANLOU & NIROUMAND, B. 2010. Synthesis and characterization of 356-SiCp composites by stir casting and compocasting methods. *Transactions of Nonferrous Metals Society China*.
SHY-WEN LAI & D.D.L. CHUNG 1994. haping metal matrix composites by thixotropic machining. *Journal of Materials Processing and Technology,* 58.
SMALLMAN, R. E. 2013. *Modern Physical Metallurgy*, Elsevier.
SMIT, J. J. A. C. 2000. *Die vervaardiging en die bepaling van die Meganiese eienskappe van vliegas-versterkte aluminium.* Masters, North West University.
SURESH, S., MORTENSEN, A. & NEEDLEMAN, A. 1993. *Fundamentals of Metal Matrix Composites*, Butterworth-Heineman.
SVEIN ODDVAR OLSEN, TORBJØRN SKALAND & HARTUNG, C. 2004. INOCULATION OF GREY AND DUCTILE IRON A COMPARISON OF NUCLEATION SITES AND SOME PRACTICAL ADVISES. 12.
T. SZYKOWNY, GIĘTKA, T., ROMANOWSKI, Ł. & TREPCZYŃSKA-ŁENT, M. 2014. A Study of Effects of Precipitation Hardening of Low-Alloy Copper-Nickel Spheroidal Cast Iron. *ISSN,* 14**,** 5.
TÂNIA NOGUEIRA FONSECA SOUZAA, NOGUEIRAC, R. A. P. S., FRANCOB, F. J. S., AGUILARD, M. T. P. & CETLINA, P. R. 2014. Mechanical and Microstructural Characterization of Nodular Cast Iron (NCI) with Niobium Additions. *Materials Research,* 17**,** 5.
THE INTERNATIONAL ORGANIZATION FOR STANDARDIZATION 1987. *Pig-irons - Definition and classification.* ISO.
VESAN, A. Ş. 2012. Solid Solution Strengthened Ductile Irons. *EN 1563 – NEW GENERATION DUCTILE IRONS* Bert Duit, Componenta Corporation.
VOROZHTSOV, S., KHRUSTALYOV, A., KHMELEVA, M. & ZHUKOV, I. Structure and Deformation Characteristics in Magnesium Alloy ZK51A Reinforced with AlN Nanoparticles. IX Polish National Conference on Applied Mechanics, 25 November 2016 2016 Bydgoszcz, Poland. American Institute of Physics.
W. ESTES JAMES & E. SPANGLER GRANT 1959. Method of producing nodular cast iron. Google Patents.
W. MASCHKE & M. JONULEIT Inoculation of Cast Iron. *ASK Chemicals***,** 8.
X LIU & M NILMANI. The effect of particle volume fraction on the mechanical properties of aluminum-fly ash MMC. *In:* ROHATGI, P. K., ed. Processing, Properties, and Applications of Cast Metal Matrix Composites, 1996 Cincinnati, Ohio. Minerals, Metals & Materials Society, 1996.
YUAN, Y. & LEE, T. R. 2013. *Surface Science Techniques*, Springer.

APPENDIX A – Tensile Specimen Dimensions

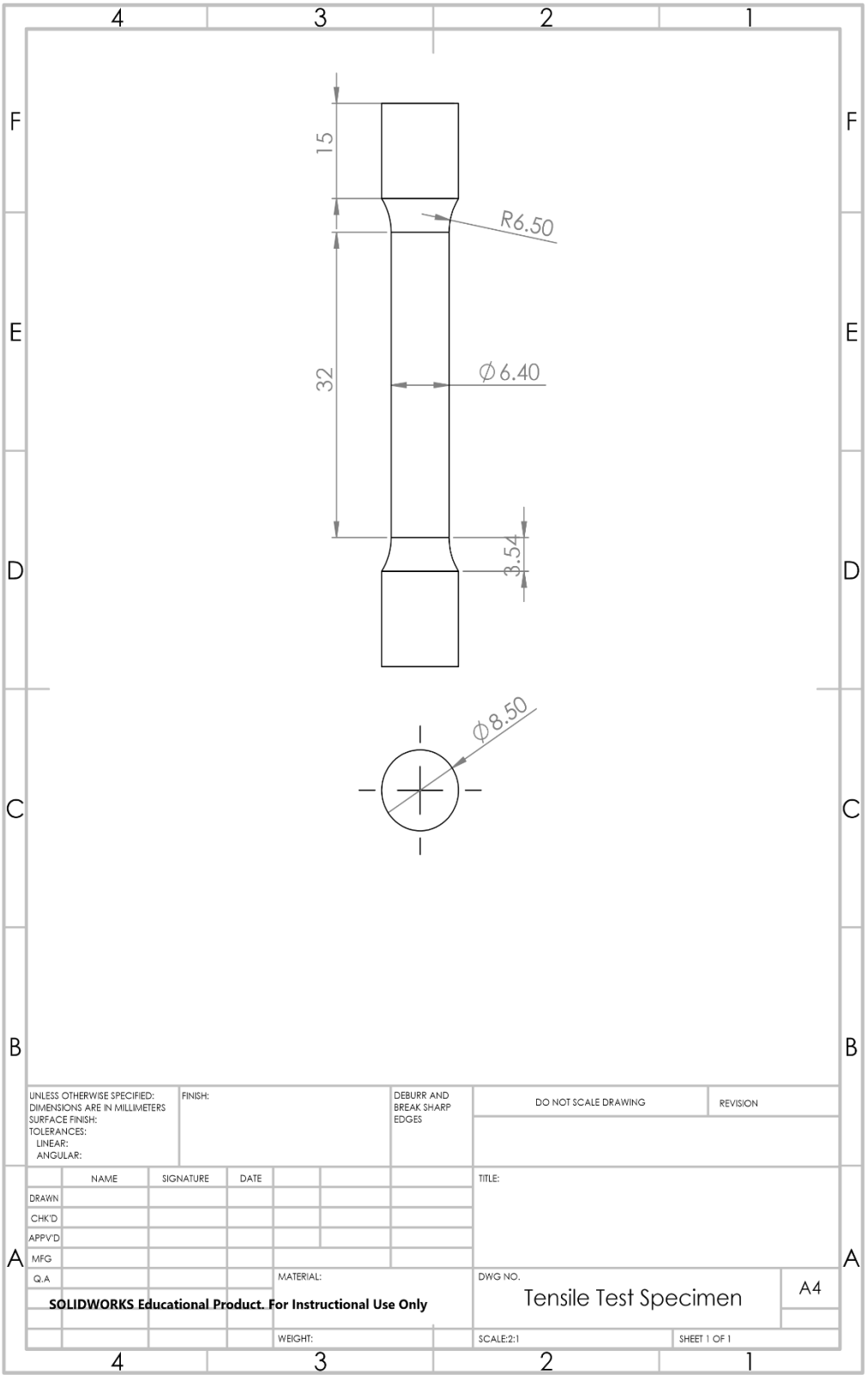

APPENDIX B – Charpy Specimen Dimensions

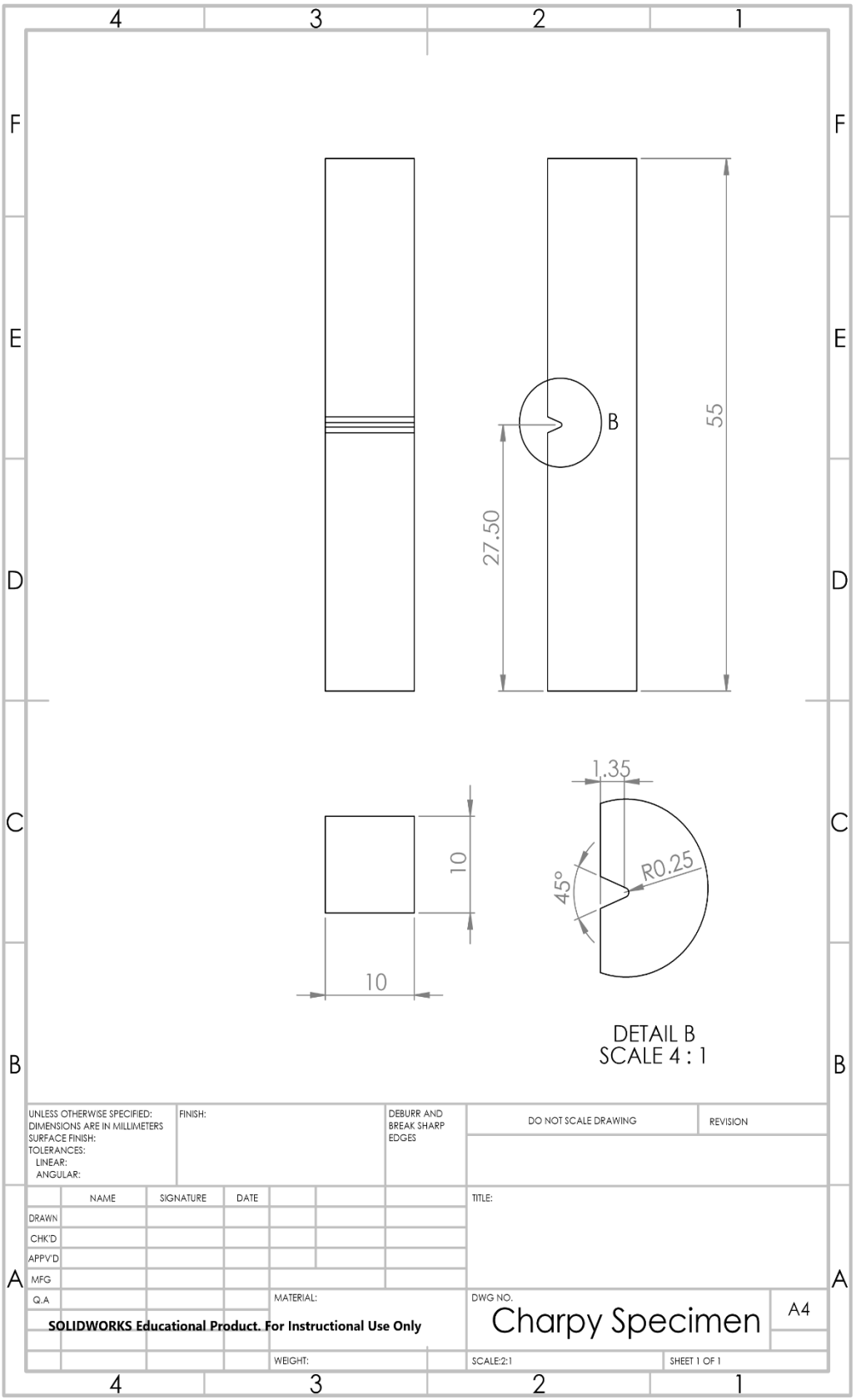

APPENDIX C – RF2 Pig Iron Composition

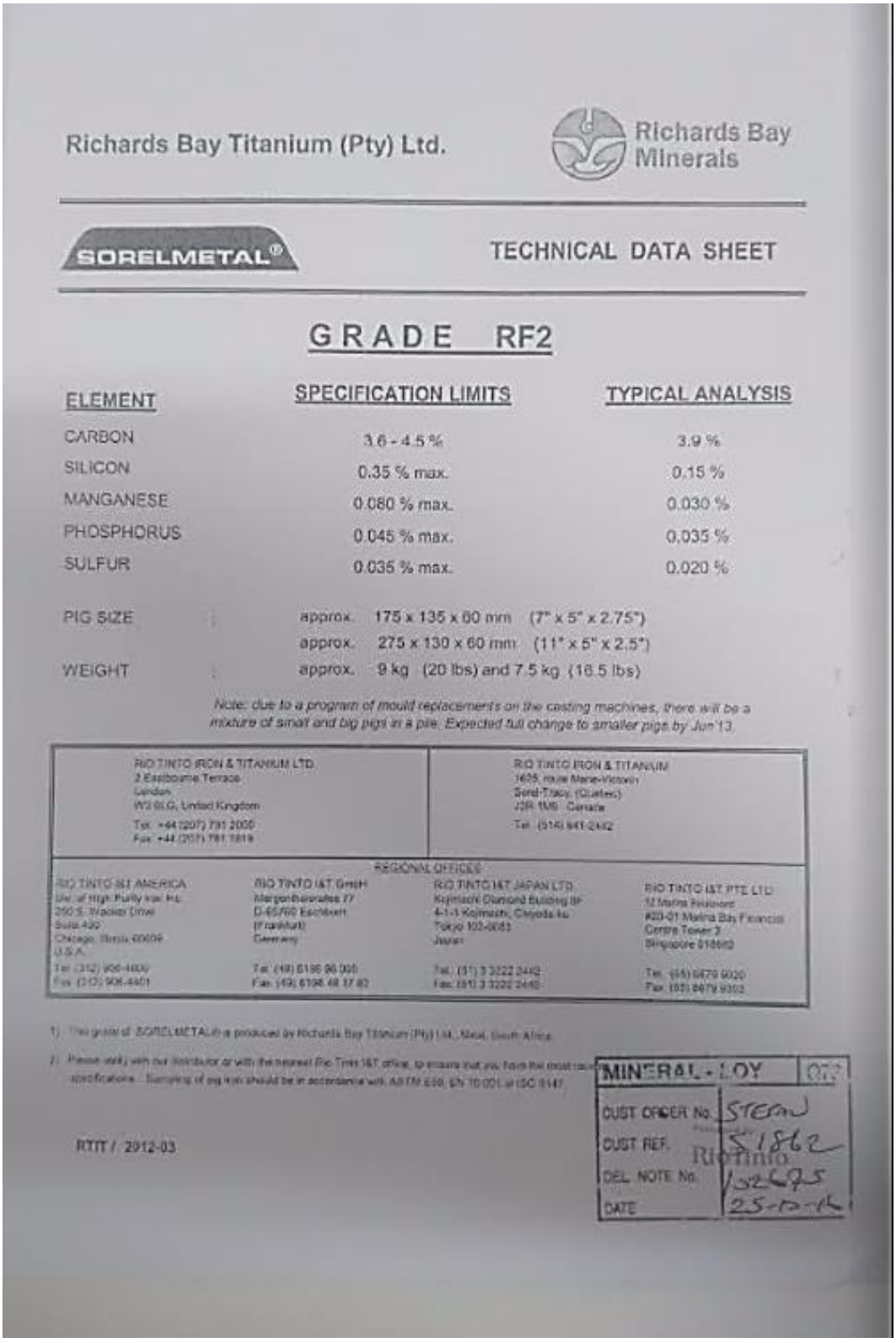

Richards Bay Titanium (Pty) Ltd.

Richards Bay Minerals

SORELMETAL®

TECHNICAL DATA SHEET

GRADE RF2

ELEMENT	SPECIFICATION LIMITS	TYPICAL ANALYSIS
CARBON	3.6 - 4.5 %	3.9 %
SILICON	0.35 % max.	0.15 %
MANGANESE	0.080 % max.	0.030 %
PHOSPHORUS	0.045 % max.	0.035 %
SULFUR	0.035 % max.	0.020 %

PIG SIZE : approx. 175 x 135 x 60 mm (7" x 5" x 2.75")
approx. 275 x 130 x 60 mm (11" x 5" x 2.5")

WEIGHT : approx. 9 kg (20 lbs) and 7.5 kg (16.5 lbs)

Note: due to a program of mould replacements on the casting machines, there will be a mixture of small and big pigs in a pile. Expected full change to smaller pigs by Jun'13.

RIO TINTO IRON & TITANIUM LTD.
2 Eastbourne Terrace
London
W2 6LG, United Kingdom
Tel: +44 (207) 781 2000
Fax: +44 (207) 781 1818

RIO TINTO IRON & TITANIUM
1625, route Marie-Victorin
Sorel-Tracy, (Quebec)
J3R 1M6 Canada
Tel: (514) 941-2442

REGIONAL OFFICES

RIO TINTO I&T AMERICA
Div. of High Purity Iron Inc.
250 S. Wacker Drive
Suite 420
Chicago, Illinois 60606
U.S.A.
Tel: (312) 906-4600
Fax: (312) 906-4601

RIO TINTO I&T GmbH
Mergenthalerallee 77
D-65760 Eschborn
(Frankfurt)
Germany
Tel: (49) 6196 96 000
Fax: (49) 6196 48 37 60

RIO TINTO I&T JAPAN LTD.
Kojimachi Diamond Building 8F
4-1-1 Kojimachi, Chiyoda-ku
Tokyo 102-0083
Japan
Tel: (81) 3 3222 2442
Fax: (81) 3 3222 2440

RIO TINTO I&T PTE LTD
12 Marina Boulevard
#23-01 Marina Bay Financial
Centre Tower 3
Singapore 018982
Tel: (65) 6879 9020
Fax: (65) 6879 9002

1) The grade of SORELMETAL® is produced by Richards Bay Titanium (Pty) Ltd., Natal, South Africa.

2) Please verify with our distributor or with the nearest Rio Tinto I&T office, to ensure that you have the most up-to-date specifications. Sampling of pig iron should be in accordance with ASTM E 59, EN 10 001 or ISO 8147.

RTIT / 2012-03

MINERALOY

CUST ORDER No. STEEN
CUST REF. 51862
DEL NOTE No. 32695
DATE 25-10-12

APPENDIX D – Ferrosilicon Composition

VAT NO. 4630176008
Registration No. 1998/014091/07

1 DORMEHL STREET
ANDERBOLT
BOKSBURG

Phone: 27 11 894 3039
Fax: 27 11 894 4185
P.O.BOX 4546
ATLASVILLE, 1465

E-Mail : mrcas@iafrica.com
www.ceramicalloy.com

Ceramic and Alloy Specialists (Pty) Ltd

CERTIFICATE OF ANALYSIS

Customer	:	
Product	:	Ferro Silicon Low Al
Form / Size	:	10 x 80mm
Packaging	:	1000kg / Bag
Order No	:	
Invoice No	:	
Batch No.	:	CS7972

Si	-	73.87	%
Al	-	0.45	%
P	-	0.037	%
S	-	0.027	%
Ca	-	0.061	%
Fe	-	Balance	%

.....
2017-11-18

APPENDIX E – Elmag Noduliser Composition

VAT NO. 4630176008
Registration No. 1998/014091/07

1 DORMEHL STREET
ANDERBOLT
BOKSBURG

Phone: 27 11 894 3039
Fax: 27 11 894 4185
P.O.BOX 4546
ATLASVILLE, 1465

E-Mail : mrcas@lafrica.com
www.ceramicalloy.com

Ceramic and Alloy Specialists (Pty) Ltd

CERTIFICATE OF ANALYSIS

Customer	:	
Product	:	Ferro Silicon Magnesium (ELMAG)
Form / Size	:	4 x 25mm
Packaging	:	1500kg / Bag
Order No	:	
Invoice No	:	
Batch No.	:	CA21625

Si	=	46.4	%
Mg	=	7.20	%
RE	=	1.20	%
Ca	=	2.47	%
Al	=	0.6	%

.....

2017-11-18

Appendix F – Excel Spreadsheet (Charge Calculation)

Composition of Constituents

	Kg	wt%	C%	Si%	P%	Mn%	Cu%	Mg%	Cr%	S%	Fe%	Ca%	Al%	Ba%	Sr%	Zr%
F2 Pig Iron			**3.900**	**0.116**	**0.035**	**0.030**	**0.000**	**0.000**	**0.000**	**0.020**	**95.899**	**0.000**	**0.000**	**0.000**	**0.000**	**0.000**
FeSi Low Al			**0.000**	**73.870**	**0.037**	**0.000**	**0.000**	**0.000**	**0.000**	**0.027**	**25.555**	**0.061**	**0.450**	**0.000**	**0.000**	**0.000**
											#####					
											#####					
SG 42 Analysis			**3.600**	**2.600**	**0.040**	**0.150**	**0.000**	**0.040**	**0.000**	**0.020**	**93.550**	**0.000**	**0.000**	**0.000**	**0.000**	**0.000**

Noduliser Analysis

% Elmag in Metal (%)	**0.8**	**Mass (kg**	**0.063**													
Elmag Analysis	Kg	wt%	C%	Si%	P%	Mn%	Cu%	Mg%	Cr%	S%	Fe%	Ca%	Al%	Ba%	Sr%	Zr%
Elkem Elmag 7311			0	46.6	0	0	0	7.2	0	0	43.13	2.47	0.6	0	0	0
Mass analysis (kg)			0.000	0.029	0.000	0.000	0.000	0.005	0.000	0.000	0.027	0.002	0.000	0.000	0.000	0.000

Inoculant Analysis (FeSi)

% Inoculant in metal (%)	**0.5**	**Mass (kg**	**0.039**													
Inoculant Analysis (FeSi)	Kg	wt%	C%	Si%	P%	Mn%	Cu%	Mg%	Cr%	S%	Fe%	Ca%	Al%	Ba%	Sr%	Zr%
Elkem Zircinoc			0	75	0	0	0	0	0	0	19.95	2.25	1.25	0	0	1.55
Mass analysis			0.000	0.030	0.000	0.000	0.000	0.000	0.000	0.000	0.008	0.001	0.000	0.000	0.000	0.001

Contribution

Base Material	**Kg**	**wt%**	**C%**	**Si%**	**P%**	**Mn%**	**Cu%**	**Mg%**	**Cr%**	**S%**	**Fe%**	**Ca%**	**Al%**	**Ba%**	**Sr%**	**Zr%**
F2 Pig Iron	**7.6**	96.293	**3.755**	**0.112**	**0.034**	**0.029**	**0.000**	**0.000**	**0.000**	**0.019**	**92.344**	**0.000**	**0.000**	**0.000**	**0.000**	**0.000**
FeSi Low Al	**0.19**	2.407	**0.000**	**1.778**	**0.001**	**0.000**	**0.000**	**0.000**	**0.000**	**0.001**	**0.615**	**0.001**	**0.011**	**0.000**	**0.000**	**0.000**
	0	0.000														
		0.000														
Treatment																
Elkem Zircinoc	0.04	0.500	**0.000**	**0.375**	**0.000**	**0.000**	**0.000**	**0.000**	**0.000**	**0.000**	**0.100**	**0.011**	**0.006**	**0.000**	**0.000**	**0.008**
Elkem Elmag 7311	0.06	0.800	**0.000**	**0.373**	**0.000**	**0.000**	**0.000**	**0.058**	**0.000**	**0.000**	**0.345**	**0.000**	**0.000**	**0.000**	**0.000**	**0.000**
	Kg	**wt%**	**C%**	**Si%**	**P%**	**Mn%**	**Cu%**	**Mg%**	**Cr%**	**S%**	**Fe%**	**Ca%**	**Al%**	**Ba%**	**Sr%**	**Zr%**
SG 42 Analysis	**7.8926039**	**100**	**3.755**	**2.638**	**0.035**	**0.029**	**0.000**	**0.058**	**0.000**	**0.020**	**93.404**	**0.013**	**0.017**	**0.000**	**0.000**	**0.008**
Required/redundant			**0.155**	**0.038**	**-0.005**	**-0.121**	**0.000**	**0.018**	**0.000**	**0.000**	**-0.146**	**0.013**	**0.017**	**0.000**	**0.000**	**0.008**

Appendix G – Spectrographic Analyses

SCROOBY'S LABORATORY SERVICE cc

Spectrographic, Chemical and Mechanical Testing of Materials

CK 1999/047204/23 | TEL: (011) 425-1074 / 0116 | P O Box 13401
21 O'Reilly Merry St | FAX: (011) 849-3571 / 086 551 6366 | Northmead
Rynfield Benoni 1501 | CELL: 082-675-4536 | 1511
VAT Reg. No: 4390188391 | CELL: 082-925-0115 | www.scroobyslab.co.za

North West University Potchefstroom
Mechanical Engineering Faculty
Building G15B
11 Hoffman Street
POTCHEFSTROOM 2531

01 November 2017

ATTENTION: Mr Stefan Louw

CERTIFICATE of ANALYSIS

REFERENCE No: **22413**

	Composition in Mass %		
ELEMENT	C	1	2
Carbon**	3.65	3.38	4.21
Manganese	0.02	0.02	≤ 0.01
Sulphur**	0.027	0.006	0.022
Phosphorus	0.016	0.028	0.048
Silicon	2.38	2.38	1.90
Chromium	0.02	0.03	0.02
Molybdenum	≤ 0.01	≤ 0.01	0.05
Nickel	0.02	0.02	0.02
Copper	≤ 0.01	≤ 0.01	≤ 0.01
Aluminium	0.019	0.009	0.018
Vanadium	≤ 0.005	0.015	≤ 0.005
Lead	≤ 0.005	≤ 0.005	0.048
Tin	≤ 0.005	≤ 0.005	0.080
Titanium	≤ 0.005	0.011	≤ 0.005
Magnesium	0.057	0.010	0.097
Iron	Matrix	Matrix	Matrix

**By combustion in oxygen method.

Description of Sample's: Mounted samples

Method #: SLS-SPC

The results relate only to the item tested.

Alan John Scrooby
2017.11.02
11:45:22 +02'00'

Technical Signatory

*Results marked ** in this report are not included in the SANAS Schedule of accreditation for Scrooby's Laboratory. Our SANAS accreditation demonstrates technical competency for Spectrographic, Dezincification of Brass and Tensile testing and the operation of a laboratory quality management system. All information in this document is given in good faith, but without warranty or guarantee of any kind whatsoever, whether implied or expressed. The original of this certificate is held at Scrooby's Laboratory Service cc for 5 years. This certificate may not be reproduced other than in full, without the written permission of Scrooby's Laboratory Service.* SAMPLES WILL BE RETAINED FOR THREE MONTHS

END OF DOCUMENT

Appendix H – Particle Size Distribution of SuperPozz Fly Ash

MASTERSIZER 2000

Result Analysis Report

Sample Name: 3 - Average Super Pozz	**SOP Name:**	**Measured:** 28 February 2017 10:09:59 AM	
Sample Source & type: Malvern	**Measured by:** micron	**Analysed:** 28 February 2017 10:10:00 AM	
Sample bulk lot ref: 195325	**Result Source:** Averaged		
Particle Name: Aluminium silicate	**Accessory Name:** Hydro 2000MU (A)	**Analysis model:** Single narrow mode (spherical)	**Sensitivity:** Enhanced
Particle RI: 1.650	**Absorption:** 0.1	**Size range:** 0.020 to 2000.000 um	**Obscuration:** 12.69 %
Dispersant Name: Water	**Dispersant RI:** 1.330	**Weighted Residual:** 4.479 %	**Result Emulation:** Off
Concentration: 0.0113 %Vol	**Span :** 3.000	**Uniformity:** 0.954	**Result units:** Volume
Specific Surface Area: 0.931 m²/g	**Surface Weighted Mean D[3,2]:** 6.442 um	**Vol. Weighted Mean D[4,3]:** 12.420 um	

d(0.1): 3.106 um d(0.5): 7.955 um d(0.9): 26.966 um

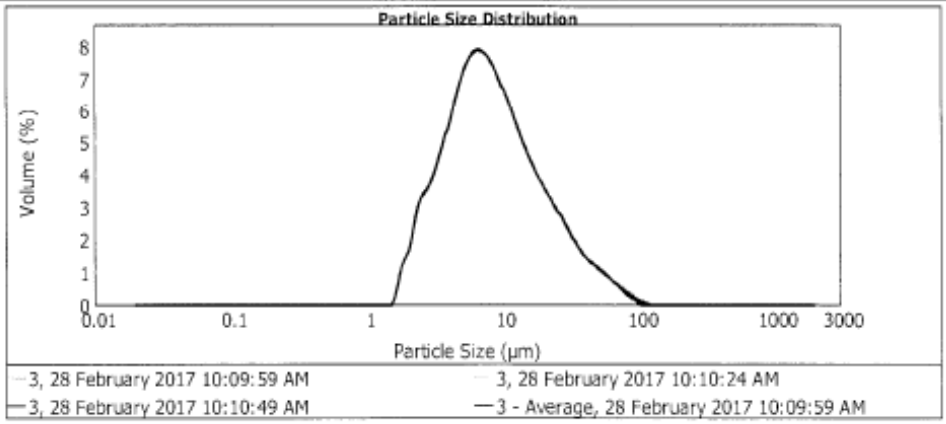

Size (µm)	Volume In %	Size (µm)	Volume In %	Size (µm)	Volume In %	Size (µm)	Volume In %	Size (µm)	Volume In %	Size (µm)	Volume In %
0.020	0.00	0.142	0.00	1.032	0.00	7.096	5.83	50.238	0.78	355.656	0.00
0.022	0.00	0.159	0.00	1.125	0.00	7.952	5.60	56.368	0.65	399.052	0.00
0.025	0.00	0.178	0.00	1.262	0.00	8.934	5.26	63.246	0.51	447.744	0.00
0.028	0.00	0.200	0.00	1.416	0.00	10.024	4.84	70.963	0.39	502.377	0.00
0.032	0.00	0.224	0.00	1.589	0.00	11.247	4.40	79.621	0.24	563.677	0.00
0.036	0.00	0.252	0.00	1.783	0.45	12.619	3.96	89.337	0.13	632.456	0.00
0.040	0.00	0.283	0.00	2.000	1.03	14.159	3.56	100.237	0.06	709.627	0.00
0.045	0.00	0.317	0.00	2.244	1.43	15.887	3.20	112.468	0.00	796.214	0.00
0.050	0.00	0.356	0.00	2.518	2.25	17.825	2.90	126.151	0.00	893.367	0.00
0.056	0.00	0.399	0.00	2.825	2.55	20.000	2.62	141.589	0.00	1002.374	0.00
0.063	0.00	0.448	0.00	3.170	2.82	22.440	2.35	158.886	0.00	1124.633	0.00
0.071	0.00	0.502	0.00	3.557	3.25	25.179	2.07	178.250	0.00	1261.915	0.00
0.080	0.00	0.564	0.00	3.991	3.80	28.251	1.77	200.000	0.00	1415.692	0.00
0.089	0.00	0.632	0.00	4.477	4.42	31.699	1.49	224.404	0.00	1588.090	0.00
0.100	0.00	0.710	0.00	5.024	5.02	35.566	1.24	251.785	0.00	1782.502	0.00
0.112	0.00	0.796	0.00	5.637	5.50	39.905	1.05	282.508	0.00	2000.000	
0.125	0.00	0.893	0.00	6.325	5.60	44.774	0.91	316.979	0.00		
0.142	0.00	1.002	0.00	7.096	5.60	50.238	0.91	355.656	0.00		

Operator notes:

Malvern Instruments Ltd.
Malvern, UK
Tel := +(44) (0) 1684-892456 Fax +(44) (0) 1684-892789

Mastersizer 2000 Ver. 5.60
Serial Number : MAL100928

File name: StefanLouw.mea
Record Number: 12
2017/03/28 10:11:34 AM